Chemical Papers (2022) 76:3705–3727
https://doi.org/10.1007/s11696-022-02123-1

ORIGINAL PAPER

Coordination behavior, structural, statistical and theoretical investigation of biologically active metal-based isatin compounds

Sajjad Hussain Sumrra[1] · Fazila Mushtaq[1] · Fayyaz Ahmad[2] · Riaz Hussain[3] · Wardha Zafar[1] · Muhammad Imran[4] · Muhammad Naveed Zafar[5]

Received: 7 September 2021 / Accepted: 4 February 2022 / Published online: 24 February 2022

Abstract

Isatin-core-containing ligands were synthesized by reacting an equimolar ratio of isatin with ethanolamine and anthranilic acid, respectively. The ligands were characterized by using FT-IR, UV–Vis, ^{1}H-NMR, ESIMS and elemental analysis. The synthesized ligands were further complexed with transition metal ions in a 1:2 molar ratio. Metal complexes were also characterized by physical, analytical and spectral methods in addition to molar conductance and magnetic moment measurements. The DFT calculations at B3LYP/6–311 + + G(d,p) level were accomplished for comparative study of isatin-based compounds. A good agreement among experimental UV–Vis, FT-IR and corresponding DFT results was found, which confirmed the purity of the studied compounds. The antimicrobial profile of all the compounds was evaluated by testing their antibacterial activity against two species of Gram-positive bacteria (*Staphylococcus aureus, Streptococcus pyogenes*) and two species of Gram-negative bacteria (*Pseudomonas syringae, Escherichia coli*) and antifungal activity against three species of fungi (*Aspergillus niger, Rhizopus stolonifer* and *Trichoderma spirale*) using the disk diffusion method. Moreover, the compounds were also investigated for antioxidant activity using phosphomolybdate and DPPH assays. The ligands revealed moderate activity against targets, which increased further upon complexation with different metal ions due to the chelation process. In addition, ANOVA and Tukey test for the experimental results of biological activities for all the prepared compounds supported the significant difference in all preclinical treatments' performance. The results showed that the isatin metal-based compounds are potent for being active as antimicrobial and antioxidant prototypes.

✉ Sajjad Hussain Sumrra
sajjadchemist@uog.edu.pk; sajjadchemist@gmail.com

[1] Department of Chemistry, University of Gujrat, Gujrat 50700, Pakistan

[2] Department of Statistics, University of Gujrat, Gujrat 50700, Pakistan

[3] Department of Chemistry, University of Education, Dera Ghazi Khan Campus, Lahore 54770, Pakistan

[4] Department of Chemistry, Faculty of Science, King Khalid University, P.O. Box 9004, Abha 61413, Saudi Arabia

[5] Department of Chemistry, Quaid-I-Azam University, Islamabad 45320, Pakistan

Graphical abstract

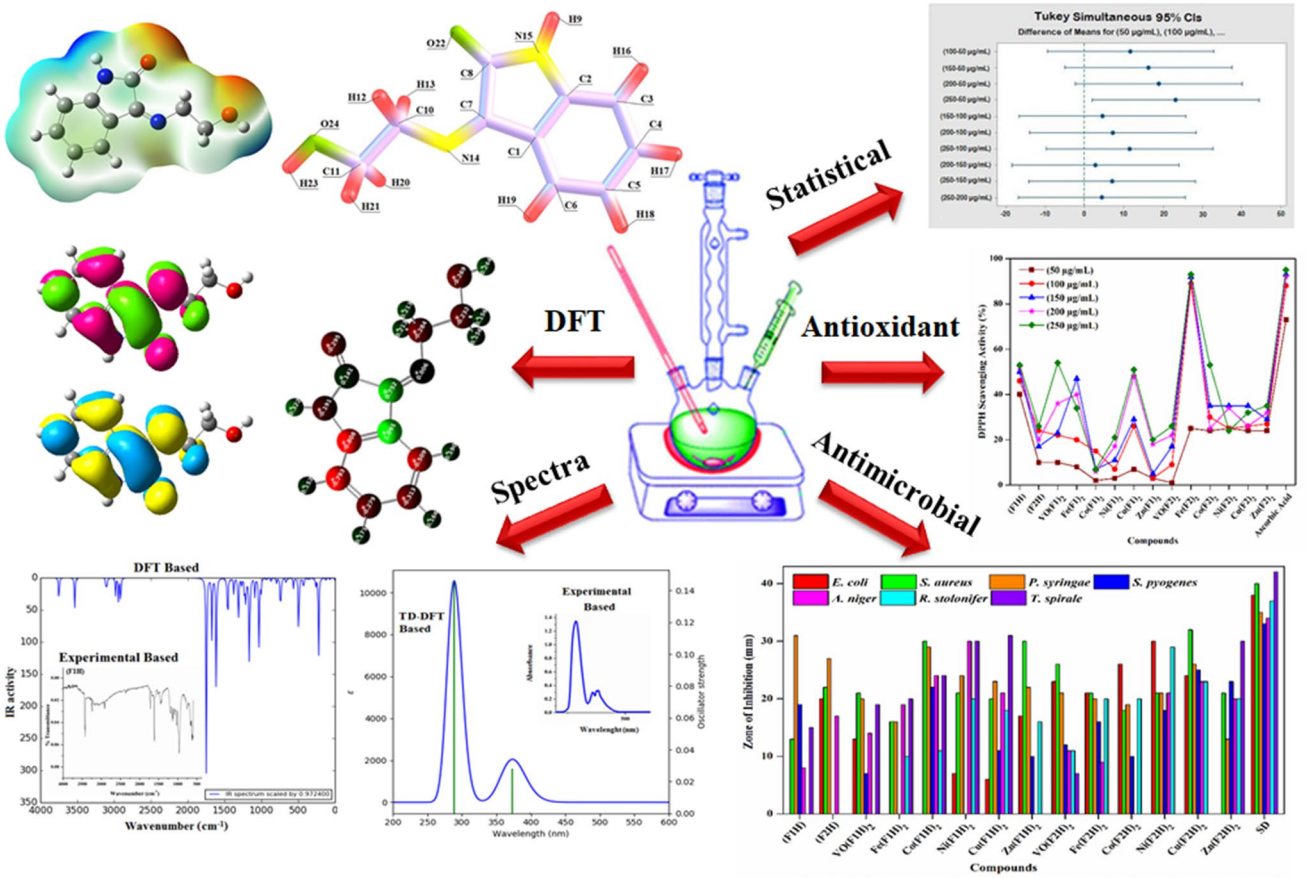

Keywords Isatin-based compounds · ANOVA · Tukey test · Antioxidant · Computational studies

Introduction

Synthetic chemistry is playing an innovative role in preparing bioactive compounds (Yakan et al. 2020). Isatin (1*H*-indol-2,3-dione) is a privileged scaffold and is one of the most important series of polyfunctional heterocyclic derivatives that exhibit versatile activity profiles and tolerated well in humans. Due to its wide range of biological activities, it has gained many promising applications in pharmaceutical chemistry (Kakkar, 2019). It is also considered as a versatile substrate for the synthesis of different isatin-based compounds, such as indoles and quinolines, and also as a starting material for drug synthesis (Havrylyuk et al. 2012). These compounds have been reported to show numerous biological activities including antibacterial (Guo 2019), antifungal (Dar et al. 2019), antiviral (De Moraes et al. 2019), anti-HIV (Li et al. 2018), anti-inflammatory (Brandão et al. 2020), anticancer (Ibrahim et al. 2016), anti-amyloid (González et al. 2009), antiulcer, antioxidant and anti-leishmanial activities (Sonmez et al. 2019). Isatin analogous was reported to display neuropharmacological and neurophysiological effects like antimycobacterial activity (Penthala et al. 2010).

Among isatin derivatives, isatin imines (Schiff bases) were found to exhibit a wide spectrum of biomedical activities. Isatin scaffold-bearing Schiff bases have also been successfully employed as ligands, thus forming complexes with numerous transition metal cations. So, over the years, the research on the metal complexes of isatin-derived Schiff-base ligands has gained much interest (Bashiri et al. 2021). The metal complexes of isatin-derived Schiff bases have exhibited multifarious progress in the pharmacological industry because of their therapeutic and diagnostic properties (Shakir et al. 2016). Out of these complexes, Cu(II) complexes of isatin imines have attracted much more consideration, mainly owing to their effective anticancer activities. Likewise, many isatin-derived imines and their respective Cu(II) complexes have also been reported in the literature to demonstrate promising antimicrobial and cytotoxic action against various cells (Pervez et al. 2016). Isatin-derived

metal complexes have also shown moderate to significant antibacterial action against various bacterial strains. Considering the antibacterial properties, mono-isatin-derived metal complexes displayed weaker activity than the bis-isatin-derived metal complexes (Guo, 2019).

Bacterial resistance is one of the most important worldwide health issues due to the multidrug resistance of pathogenic species (Kaur et al. 2010). Currently, the design, study and synthesis of biologically active metal-based chelates from Schiff base ligands with nitrogen and oxygen donor atoms are one of the embryonic areas of research owing to their competent pharmacological actions (Sumrra et al. 2021a, b, c; Ejidike and Ajibade 2015). Predominantly, the Schiff base ligands possessing nucleophilic substituents such as –OH, –SH and $–NH_2$ at *ortho* position to the imine linkage were found to be more appropriate for complexation with transition metal cations, thus producing more stable metal chelates (Sumrra et al. 2021a, b, c). These types of nitrogen- and oxygen-coordinated metal complexes are widely studied due to their excellent biological and physicochemical properties (Sakthikumar et al. 2019). They are predominant among the type of compounds used as pharmaceuticals (Dharsini et al. 2020), antioxidants, sensitizers and dyestuff (Ejidike and Ajibade 2016). They are significant topics of structural and synthetic research due to their structural versatility (Pedreño et al. 2005), easy synthetic approach and more significant biological activity than the non-coordinated ligands (Nagesh and Mruthyunjayaswamy 2015).

The reactivity of transition metal chelates is influenced by the type of coordinating ligands, the oxidation state of the central metal ion and the coordination geometry of the metal complexes (Sumrra et al. 2020). Existing antibiotic resistance is one of the leading sources of motivation to develop and explore new effective agents for inhibiting bacterial growth (Mitra et al. 2013). The metal ions complexed with bioactive agents are more effectual, for the reason that both the components (ligands and metal ions) have the potential to affect various stages of pathogenic life cycles. In most cases, metal complexes are capable of catalyzing life-sustaining metabolic reactions. The metallic part of the complex is typically responsible for effectively binding with DNA, thus damaging the vital genetic material of microbes (Zafar et al. 2021).

Recently, the quantum chemical approaches established on density functional theory (DFT) have been credibly used to accelerate the high throughput drug screening (Akman et al. 2020). These computational methodologies have been acknowledged for their accuracy and efficiency when it comes to predict and understand the electronic structure of newly synthesized compounds to correlate their experimentally observed structural features (Sagaama et al. 2020). The chemical reactivity of molecules was predicted by employing the frontier molecular orbitals (FMOs) accompanied by eminent descriptors (Jomaa et al. 2020). Moreover, various electronic properties including FMO energy gaps and absorption wavelengths together with oscillator strengths have been calculated through TD-DFT method (Issa et al. 2020).

In continuance of our previous work concerning metal-based isatin compounds (Khalid et al. 2020), in the work reported here we aimed to synthesize some more divalent and tetravalent complexes with our target isatin-based ligands. Spectral characterization and molecular modeling were employed for the structural elucidation of synthesized compounds. Theoretic studies using DFT and time-dependent DFT computations have been executed and combined with experimental results throughout this work for structural, electronic and vibratory characterization. The biological activity of synthesized compounds with moderate to significant biological interactions was explored by their FMO energies gaps. In vitro biological activities were performed to study the antimicrobial and antioxidant activity profile of all the compounds. According to the results, all the studied compounds were found to have therapeutic potential and exhibited exciting properties from the pharmacological aspect which will ultimately prove the capability of these active components in new medicinal products.

Experimental

All the required chemicals were ordered from Merck, Sigma–Aldrich (A.R), and consumed as received without additional refinement. Stuart apparatus was utilized to measure the melting points of all compounds. Infrared spectra were collected using a Nicolet, iS5 FT-IR spectrophotometer in the working range of 4000–400 cm^{-1}. UV–Vis spectra were recorded on a Hitachi UV-3200 spectrophotometer using DMF (dimethylformamide)-based solutions. The C, H and N analysis was performed on a high tech, 2400 CHN elemental analyzer. ^{1}H-NMR spectra were documented on a 300 MHz Bruker instrument. For the electron impact mass spectrometric analysis, the isatin compounds (including the ligands and their complexes) were dissolved in methanol and inserted directly by the use of a direct insertion pump into the LTQ XL linear ion trap mass spectrometer (Thermo Scientific, USA) fitted out with an electrospray ionization (ESI) probe. Capillary temperature was fixed at 350 °C, while the flow of sheath gas (N_2) at 30 arbitrary units. All the samples were analyzed in both modes: positive- and negative-ion mode with a 10-µL/min flow rate. Then, the data were collected at both types of full-scan modes with a mass scan *m/z* ranging from 50 to 700 using Xcalibur software.

By using the full-scan ESI–mass spectra, the synthesized compounds were characterized. ESI–MS gave detailed *m/z*

Scheme 1 Synthesis of isatin-derived Schiff bases **(F1H)** and **(F2H)**

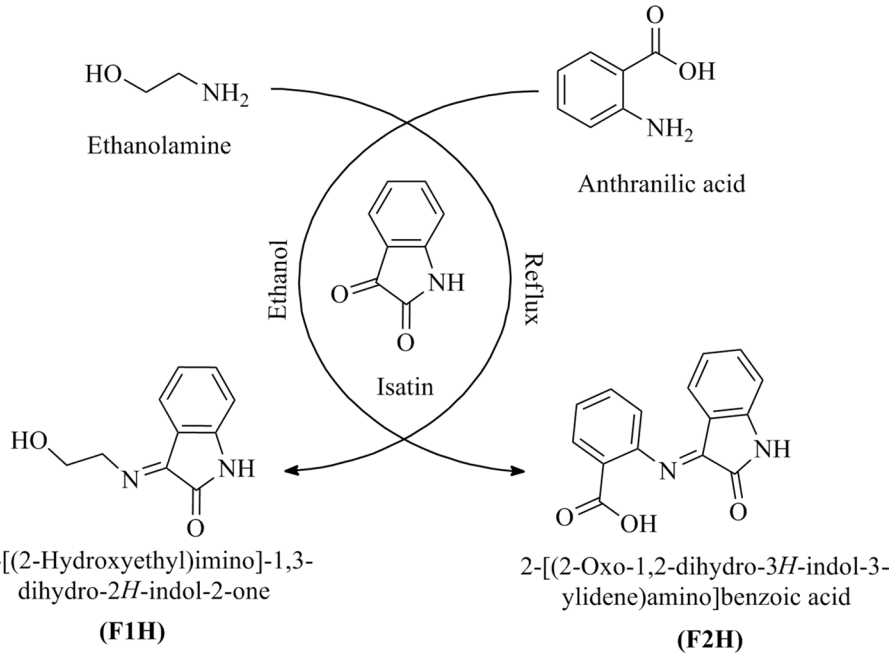

peaks by making $[M+Na]^+$, $[M\text{-}H]^-$ and $[M+H]^+$ ions. The ESI–MS/MS fragmentation pattern of the known peaks was utilized to further fragment the daughter ions to confirm the molecular identity of each ligand and complex. Molar conductivity of synthesized complexes was determined by the use of Inolab Cond 720 Conductivity Bridge at room temperature with 0.001 molar DMF-based solutions. The magnetic susceptibility of the synthesized complexes was executed with the magnetic susceptibility balance (MSB) (Mk1 design) using $MnCl_2$ as standard.

Synthesis of ligands (F1H) & (F2H)

The isatin-based ligands, namely 3-[(2-hydroxyethyl)imino]-1,3-dihydro-2*H*-indol-2-one **(F1H)** and 2-{[2-oxo-1,2-dihydro-3*H*-indol-3-ylidene]amino}benzoicacid **(F2H),** were prepared by implementing a previously described protocol (Arunachalam et al. 2010) as shown in Scheme 1. For the synthesis of ligand **(F1H)**, to the refluxed ethanolic solution of isatin (1.47 g, 10 mmol) in a double-neck flask, the solution of ethanolamine (0.60 mL, 10 mmol) was added with constant stirring after 1 h of refluxing. The reaction progression was continuously noted through TLC (thin-layer chromatography). The precipitates obtained after 21 h were cooled at room temperature, followed with filtration, washed with boiling ethanol and then recrystallized in an equimolar mixture of ether and ethanol to get pure product. Similarly, the other ligand **(F2H)** was synthesized with the same protocol by using anthranilic acid instead of ethanolamine.

3-[(2-Hydroxyethyl) imino]-1,3-dihydro-2*H*-indol-2-one (F1H)

Yield (%): 65; m.p (°C): 126; color: dark brown; IR (cm^{-1}): 3420 (OH), 3241 (NH), 1715 (C = O), 1644 (C = N); ^{1}H-NMR (DMSO-d_6) δ ppm: 3.34–3.99 (t, aliphatic protons), 7.62 (s, 1H, NH), 6.75–7.64 (m, aromatic protons), 4.02 (s, 1H, OH); ESIMS *m/z* (%): 163.92 (100), 147.92 (58), 174.00 (56), 191.92 (38), 180.42 (8), 131.00 (6), 118.92 (2); Anal. Calcd. (%) for $C_{10}H_{10}N_2O_2$; 190.1: calculated; C 63.15, H 5.30, N 14.73: found; C 63.07, H 5.27, N 14.69.

2-{[2-Oxo-1,2-dihydro-3*H*-indol-3-ylidene] amino}benzoicacid (F2H)

Yield (%): 77; m.p (°C): 185; color: dark orange; IR (cm^{-1}): 3389 (OH), 3220 (NH), 1710 (C = O), 1632 (C = N); ^{1}H-NMR (DMSO-d_6) δ ppm: 11.04 (s, 1H, OH), 7.51 (s, 1H, NH), 6.89–7.62 (m, aromatic protons); ESIMS *m/z* (%): 266.25 (100), 205.17 (28), 179.17 (20), 146.08 (10), 247.25 (5), 136.08 (4), 118.00 (2); Anal. Calcd. (%) for $C_{15}H_{10}N_2O_3$; 266.3: calculated; C 67.67, H 3.79, N 10.52: found; C 67.51, H 3.68, N 10.41.

Synthesis of metal complexes

The ethanolic solution of respective metal salt [hydrated iron(II) sulfate, cobalt(II) chloride, nickel(II) chloride, copper(II) chloride, zinc(II) chloride and vanadyl(IV)

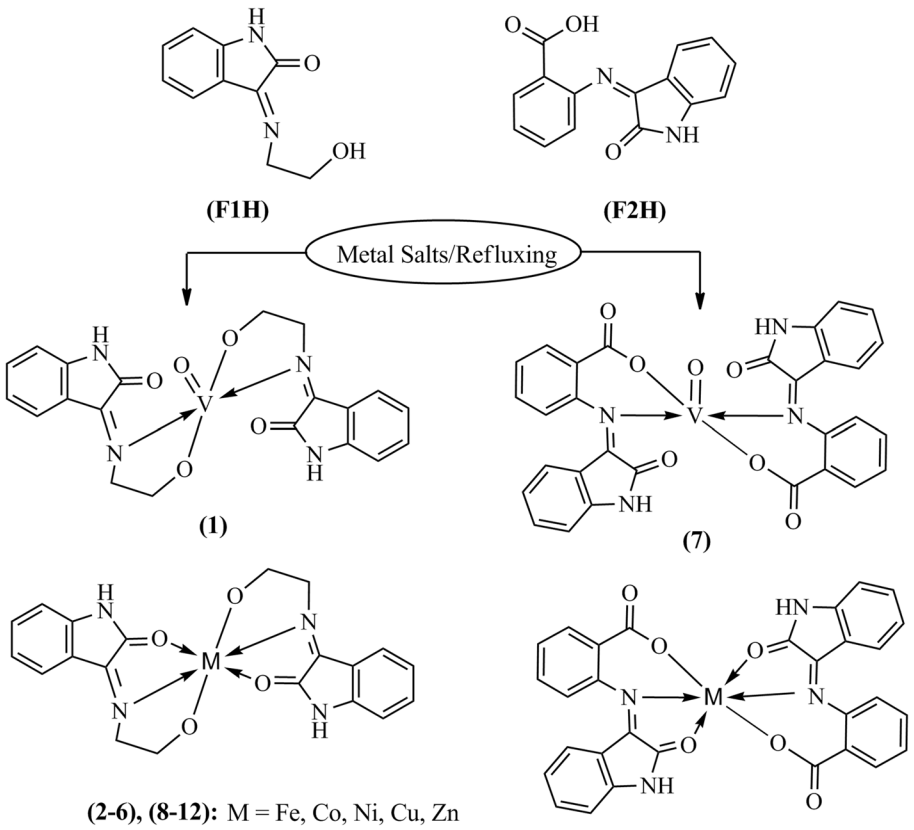

Scheme 2 Synthesis of metal-based isatin-derived Schiff base compounds **(1)–(12)**

sulfate] (0.5 mmol) was added to the magnetically refluxing ethanolic solution of isatin-based ligand (1 mmol) in two neck flask, after 1 h of refluxing (Scheme 2). The reaction progress was continuously checked through TLC. The recovered precipitates of the product were cooled at room temperature, followed with filtration, washed with hot ethanol and afterward recrystallized in the equimolar mixture of ether and ethanol.

Antimicrobial activity

Antibacterial activity

All the synthesized ligands and their derived 3*d*-metal complexes have been tested for antibacterial activity using two species of Gram-positive bacteria (*S. aureus, S. pyogenes*) and two species of Gram-negative bacteria (*P. syringae, E. coli*) by disk diffusion test (Sumrra et al. 2016). The nutrient broth, petri plates and filter paper strips were autoclaved at 121 °C for half an hour. Partially liquid agar media were distributed to petri plates and allowed to solidify; then, the bacterial inoculum was dispersed on the media using a glass spreader. Round strips of filter paper were arranged on the media, and 20 µL sample (25 mg/mL concentration in DMSO solvent) was injected on disks using a micropipette. Amoxicillin was used as a standard in this procedure. Then, the petri plates were stacked in an incubator at 37 °C and the inhibition zone was measured in millimeter after 48 h.

Antifungal activity

Newly prepared isatin-based ligands and their complexes were checked for in vitro antifungal activity against three fungal strains (*A. niger, R. stolonifer* and *T. spirale*) by disk diffusion test (Sumrra et al. 2016). The media (prepared by adding 2 g glucose, 2 g agar, 0.02 g potassium dihydrogen phosphate, 0.005 g magnesium sulfate, 0.005 g calcium chloride and 0.02 g ammonium sulfate), petri plates and filter paper strips were autoclaved at 121 °C for half an hour. Semi-liquid media were distributed to petri plates and left for setting; then, the fungal inoculum was dispersed on the media using a glass spreader. Round strips of filter paper were arranged on the media, and 20 µL sample (25 mg/mL concentration in DMSO solvent) was injected onto disks using a micropipette. Fungom was used as a standard in this procedure. Then, the petri plates were stacked in an incubator at 37 °C and the inhibition zone was measured in millimeter after 48 h.

Antioxidant activity

Antioxidant activity of prepared compounds was determined using two methods, *i.e.,* DPPH and phosphomolybdate assays.

DPPH method

Antioxidant activity of prepared compounds was checked through the recommended procedure using DPPH (2,2-diphenyl-1-picrylhydrazyl) radical (Bakır and Lawag 2020). Five different concentration levels (50, 100, 150, 200 and 250 µg/mL) of the compounds and ascorbic acid (standard) were prepared, which were then poured in the test tubes and mixed with freshly prepared DPPH (2 mL, 2 mM) solution and then kept in the dark for half an hour. After that, the absorbance of compounds and standard was noted at 517 nm wavelength, and the percentage inhibition was quantified by using the following formula (Eq. 1).

$$Percentage\,(\%)\,inhibition = \frac{(Blank - Sample)}{Blank} \times 100. \quad (1)$$

Phosphomolybdate method

The total antioxidant capacity of isatin-derived Schiff bases **(F1H)** and **(F2H)** as well as their metal chelates was determined through the recommended procedure (Sumrra et al. 2018). Respective compound solution (0.2 mL) was poured in reagent solution (2 mL) that was prepared through intermingling sodium phosphate (28 mM), ammonium molybdate $(NH_4)_2MoO_4$ (4 mM) and 0.1 M H_2SO_4 (5 mL). This mixture was warmed up to 95 °C temperature for 35 min, and the absorbance reading was then noted at 695 nm wavelength using UV–Vis spectrophotometer.

Statistical analysis

The statistical analysis was accomplished by the use of Minitab software (Keeling and Pavur, 2007) to interpret the experimental outcomes of biological studies, including antibacterial, antifungal and antioxidant activities.

Computational details

Computational calculations of the investigated isatin-derived ligands **(F1H)** and **(F2H)** as well as their selected metal complexes were accomplished by DFT using B3LYP (Becke, 3 parameters, Lee–Yang–Parr) level of theory in combination with basis set 6–311 + + G(d,p) through Gaussian 09 D.0.1 package (Frisch et al. 2009). The B3LYP functional is the modified version of the Becke hybrid functional and is most commonly used hybrid functional. All the input data files of the studied compounds were obtained by using GaussView software (Dennington et al. 2009).

In DFT calculations, at the start, the geometries of all the studied compounds were completely optimized by employing DFT/B3LYP in combination with 6–311 + + G(d,p) basis set. After that, using the frequency calculations at the same basis set, the stability profile was confirmed for all the optimized geometrical structures. The lack of negative eigenvalues out of all the computed frequencies signified proper minimal level of their potential energy surfaces.

Neutral structures of all the investigated compounds were obtained after optimization of their geometries. The UV–visible analysis was accomplished using TD-DFT with B3LYP/6–311 + + G(d,p) (Brémond et al. 2010). The IR, FMO, NBO, MEP and MAC calculations were done on these optimized geometries by the use of same settings. Finally, the output data were interpreted by means of Chemcraft, GaussView, Avogadro and GaussSum programs.

Results and discussion

Physical characterization

The isatin Schiff base ligands **(F1H)** and **(F2H)** have been prepared by the condensation reaction of isatin moiety with ethanolamine and anthranilic acid, respectively, in an equimolar ratio using ethanol as solvent. The prepared isatin-based ligands were complexed with metallic cations of vanadium, iron, cobalt, nickel, copper and zinc. All the compounds were stable in air and moisture. All the compounds were synthesized with a good yield ranging from 62 to 84%. Melting points of ligands and decomposition points of complexes provided a strong indication about the formation of both ligands and their resultant metal complexes.

All the 3*d*-metal chelates were obtained in intense colors except zinc complexes. They were completely

Table 1 Physical, elemental and analytical characteristics of synthesized compounds

Compound Color	Yield/% M.P/°C	M.W/gmol^{-1} Formula	Calculated (Present)/%			
			C	H	N	M
(F1H) Dark brown	65 126	[190.19] $C_{10}H_{10}N_2O_2$	63.15 (63.07)	5.30 (5.27)	14.73 (14.69)	–
(F2H) Dark orange	77 185	[266.25] $C_{15}H_{10}N_2O_3$	67.67 (67.59)	3.79 (3.73)	10.52 (10.45)	–
$VO(F1)_2$ Green	71 > 300	[445.32] $C_{20}H_{18}N_4O_4VO$	53.94 (53.85)	4.07 (4.02)	12.58 (12.55)	11.44 (11.39)
$Fe(F1)_2$ Light green	62 266	[434.22] $C_{20}H_{18}N_4O_4Fe$	55.32 (55.27)	4.18 (4.14)	12.90 (12.88)	12.86 (12.81)
$Co(F1)_2$ Brown	77 171	[437.31] $C_{20}H_{18}N_4O_4Co$	54.93 (54.89)	4.15 (4.11)	12.81 (12.78)	13.48 (13.42)
$Ni(F1)_2$ Light brown	69 > 300	[437.07] $C_{20}H_{18}N_4O_4Ni$	54.96 (54.91)	4.15 (4.13)	12.82 (12.73)	13.43 (13.38)
$Cu(F1)_2$ Dark green	63 > 300	[441.92] $C_{20}H_{18}N_4O_4Cu$	54.36 (54.33)	4.11 (4.06)	12.68 (12.61)	14.38 (14.33)
$Zn(F1)_2$ Off white	84 213	[443.79] $C_{20}H_{18}N_4O_4Zn$	54.13 (54.09)	4.09 (4.02)	12.62 (12.58)	14.74 (14.69)
$VO(F2)_2$ Light green	73 287	[597.43] $C_{30}H_{18}N_4O_7V$	60.31 (60.22)	3.04 (3.01)	9.38 (9.32)	8.53 (8.45)
$Fe(F2)_2$ Green	76 293	[586.33] $C_{30}H_{18}N_4O_6Fe$	61.45 (61.37)	3.09 (3.03)	9.56 (9.53)	9.52 (9.43)
$Co(F2)_2$ Brown	74 > 300	[589.42] $C_{30}H_{18}N_4O_6Co$	61.13 (61.08)	3.08 (3.01)	9.51 (9.46)	10.00 (9.97)
$Ni(F2)_2$ Light orange	81 > 300	[589.18] $C_{30}H_{18}N_4O_6Ni$	61.16 (61.12)	3.08 (3.06)	9.51 (9.42)	9.96 (9.91)
$Cu(F2)_2$ Brick red	80 > 300	[594.03] $C_{30}H_{18}N_4O_6Cu$	60.66 (60.57)	3.05 (3.04)	9.43 (9.38)	10.70 (10.64)
$Zn(F2)_2$ Off white	75 244	[595.87] $C_{30}H_{18}N_4O_6Zn$	60.47 (60.35)	3.04 (3.02)	9.40 (9.33)	10.97 (10.93)

soluble in ethanol (EtOH), methanol (MeOH), dimethyl sulfoxide (DMSO) and dimethylformamide (DMF), but moderately soluble in other organic solvents. The proposed CHN data showed high agreement with the practically observed data. The data of elemental analysis together with some physical properties for all the compounds are depicted in Table 1.

Spectral characterization

The ligands were spectrally characterized through ^{1}H-NMR, FT-IR, UV–Vis and mass spectrometry. The experimental IR and UV–Vis results of the both isatin ligands and their selected metal complexes have also been compared with theoretical findings obtained by DFT calculations. But the complexes were also characterized using conductance and magnetic moment values.

FT-IR spectral characterization

The formation of these two Schiff bases **(F1H)** and **(F2H)** was proven from the absence of (NH_2) and (C = O) peaks in their spectra. The experimental IR spectra of isatin-based ligands showed characteristic bands of (C = N) at 1632–1644 cm^{-1} that gave a strong intimation about the condensation of reactants (Ismail et al. 2021). Both ligands also exhibited bands at 1710–1715, 3110–3191, 3220–3241 and 3389–3420 cm^{-1} due to ν(C = O), ν(C–H), ν(NH) and ν(OH) groups, respectively. With the purpose of determining the involvement of coordinating sites in chelate formation, the IR spectral data of complexes were studied in comparison with free ligands. The IR data for all the synthesized metal complexes showed the appearance of some new peaks along with the disappearance

and shifting of some already existing peaks that gave a clue about metal and ligand coordination, as depicted in Table S1 and Figs. S1–S3.

The disappearance of (OH) peaks at 3389–3420 cm^{-1} of ligands and downward shifting of v(C–O) peak from 1389–1390 to 1362–1387 cm^{-1} signified the coordination of isatin-based ligands with metal cations through deprotonated oxygen atom of the hydroxyl group (Ouari et al. 2015). For complexes, a new peak was observed in the range of 448–491 cm^{-1} owing to ν(M–O) that confirmed the metal–ligand bond through oxygen (Al-Hazmi et al. 2020). The bonding action of azomethine–nitrogen with metal cations was supported by the downward shift of frequency from 1632–1644 cm^{-1} to 1610–1631 cm^{-1} in all metal chelates. Another new peak was also observed ranging from 517 to 532 cm^{-1} because of ν(M–N) that showed the formation of metal–ligand bond through nitrogen (Chohan et al. 2010). For the vanadium complexes of both ligands, a new peak was observed at 840 and 869 cm^{-1}, respectively, indicating $\nu(V=O)$ vibration (Grivani et al. 2012). All these signals supported the coordinating action of metal ions with the isatin-derived ligands.

UV–Vis spectral characterization

The electronic spectra of isatin-based compounds have been taken in DMF solutions (10^{-1} M) in the scan range of 200–800 nm. The UV–Vis spectra of ligands **(F1H)** and **(F2H)** demonstrated two and three absorption bands 289 and 400 nm and 250, 400 and 490 nm because of π–π* and n–π* electronic transitions, correspondingly. In the metal complexes, new bands supported the formation of strong (M–N) and (M–O) bonds. The vanadyl(IV) complexes have exhibited their representative bands at 378–385, 542–554 and 749–768 nm which ascribed to the $B_2 \rightarrow E_\pi$, $B_2 \rightarrow B_1$ and $B_2 \rightarrow A_1$ electronic transitions, respectively. The high-intensity bands as a result of charge transfer from metal to ligand were observed at 327–334 nm. All these transitions signified the square pyramidal environment around VO(IV) ions. The Fe(II) complexes have shown their two representative electronic transitions comprising ^5E_g and $^5T_{2g}$ at 376–383 and 512–532 nm, approved their octahedral configuration.

The low-energy electronic bands of Co(II) complexes at 512–546 and 639–662 nm due to $^4T_{1g}(F) \rightarrow {}^4T_{1g}(P)$ and $^4T_{1g}(F) \rightarrow {}^4T_{2g}(F)$ electronic transitions together with a band of high energy at 344–352 nm attributable to metal to ligand charge transfer (MLCT), signified their high spin octahedral geometry (Kargar et al. 2021). Similarly, for Ni(II) complexes, three absorption bands appeared at 387–419, 604–627 and 765–782 nm as a result of $^3T_{2g}(F) \rightarrow {}^3T_{1g}(P)$, $^3A_{2g}(F) \rightarrow {}^3T_{1g}(F)$ and $^3A_{2g}(F) \rightarrow {}^3T_{2g}(F)$ electronic transitions, while the most intense band of MLCT was found at 329–336 nm, thus evidencing their octahedral geometry. The octahedral geometry for Cu(II) complexes was confirmed owing to the occurrence of two electronic transitions reflecting $^2B_{1g} \rightarrow {}^2E_g$ and $^2B_{1g} \rightarrow {}^2A_{1g}$ excitations at 517–529 and 631–648 nm, correspondingly, while the third band due to MLCT having high intensity was obtained at 337–342. For Zn(II) complexes, only a strong band was obtained for MLCT at 324–339 nm owing to their diamagnetic nature (Hassan and Sumrra 2021).

^{1}H-NMR spectral characterization

The ^{1}H-NMR spectra of both isatin-based ligands **(F1H)** and **(F2H)** were documented using DMSO-d_6 as a solvent. The examination of spectra showed the characteristic peak of N–H proton at 7.51–7.62 ppm as a singlet. The aromatic protons of both ligands were observed as a multiplet at 6.75–7.64 ppm. The O–H proton of ligands was obtained at 4.02 and 11.04 ppm, respectively. For ligand **(F1H)**, two signals were also observed as a triplet at 3.34–3.99 ppm for aliphatic protons of ethanolamine. All the observed signals supported the formation of both ligands and their proposed structures, as shown in Figs. S4 and S5.

Mass spectral characterization

Mass spectra of ligands **(F1H)** and **(F2H)**, as well as vanadium and zinc complexes of ligand **(F2H)**, showed various peaks at different intensities indicating molecular ion peaks, base peaks and other fragments (Table S2). For ligands **(F1H)** and **(F2H)**, **t**he molecular ion peaks appeared at $m/z = 191.92$ and 266.25, correspondingly that confirmed the formation of ligands (Figs. S6 and S7). The fragmentation design of isatin-based ligands showed the C–C, C = C and C = N bond breaking. The base peak and molecular ion peak of ligand **(F2H)** were found at the same fragment. But for ligand **(F1H)**, the highly intense base peak was found at $m/z = 163.92$. All the peaks confirmed the formation of both ligands. The proposed structures of metal complexes were also confirmed through the mass spectra as depicted in Figs. S8 and S9. The complex **$VO(F2)_2$** exhibited a molecular ion peak at $m/z = 598.00$, while the base peak at $m/z = 388.17$. Similarly, the molecular ion peak for **$Zn(F2)_2$** complex was observed at $m/z = 627.17$, whereas the most intense and stable peak was determined at $m/z = 266.25$.

Molar conductance and magnetic moments

Measurement of molar conductance for all the metal chelates was performed in DMF solvent. The results of molar conductance (11.8–19.3 $\Omega^{-1}cm^2mol^{-1}$) displayed the non-conductor identity of the metal complexes.

The magnetic moments of all synthesized chelates were determined by magnetic susceptibility balance (Table S1). The copper and vanadium complexes showed magnetic moment values ranging from 1.72 to 1.93 BM, indicating the occurrence of one unpaired electron (Maurya et al. 2015). The measured magnetic moments of cobalt complexes were found to be 4.21–4.33 BM, which showed the existence of three unpaired electrons. The nickel complexes displayed a magnetic moment at 3.01–3.15 BM, revealing the occurrence of two unpaired electrons (Hanif and Chohan 2013). The magnetic moments of the iron complexes were found to be 5.03–5.07 BM, showing the presence of four unpaired electrons in the d-orbital. The zinc complexes showed zero magnetic moment value that

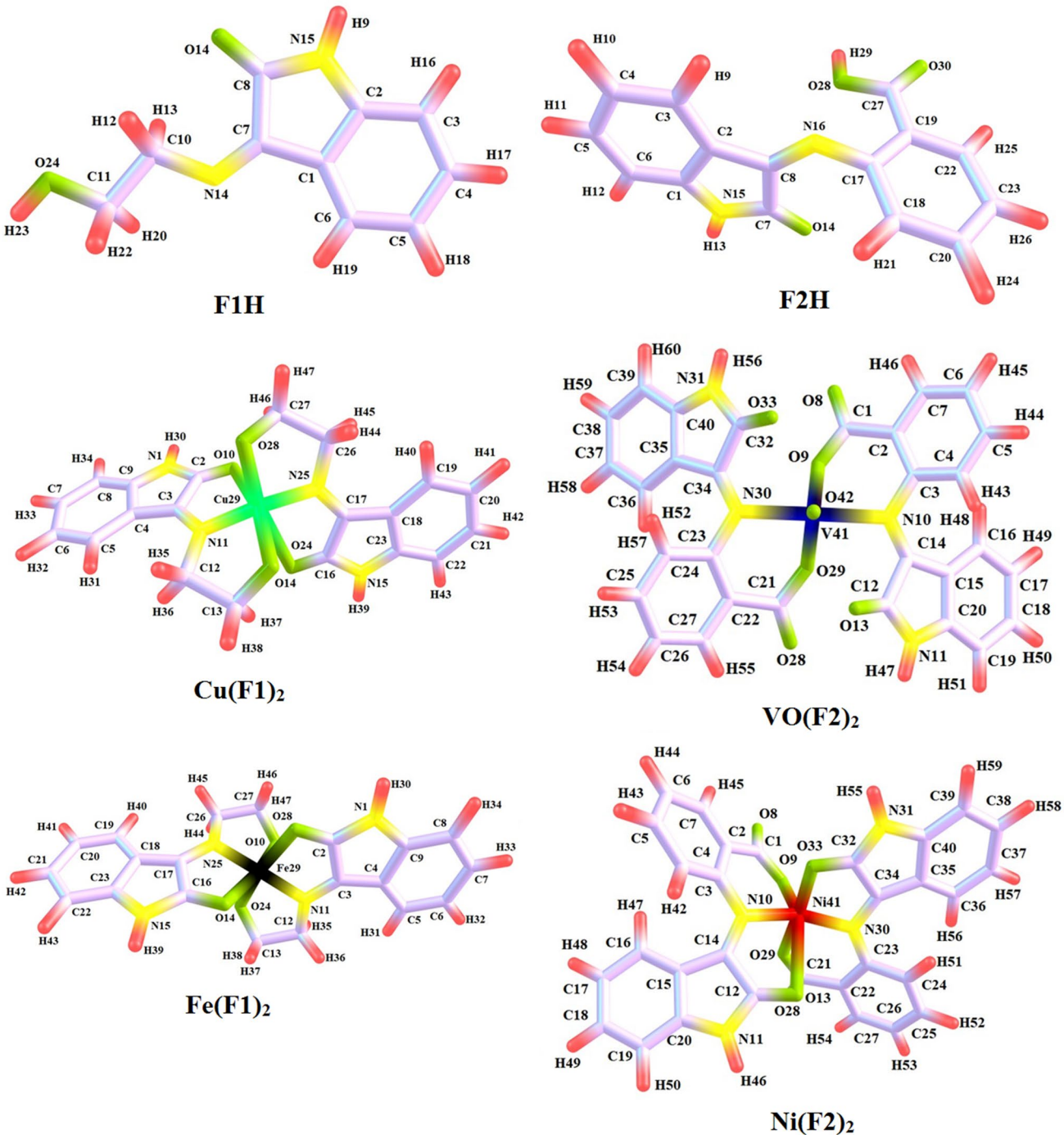

Fig. 1 Optimized structures of isatin-based compounds

indicated the diamagnetic nature of these complexes due to the d^{10} system (Chandrasekar et al. 2021). The data of molar conductance and magnetic moments of the metal complexes supported the suggested structures of the metal complexes.

Geometry optimization

The optimized geometrical structures of the both isatin-derived ligands and their selective metal chelates were visualized through Chemcraft software. Figure 1 illustrates the molecular geometries for all the compounds together with their atom numbering.

Table 2 Energies of frontier molecular orbitals and computed global reactivity descriptors for isatin-based compounds and reference compounds

Compounds	Descriptors/eV									
	E_{LUMO}	E_{HOMO}	$\Delta E_{H\rightarrow L}$	(*IP*)	(*EA*)	(η)	(μ)	(σ)	(χ)	(ω)
(F1H)	−2.548	−6.540	3.992	6.540	2.548	1.996	−4.544	0.250	4.544	5.170
(F2H)	−2.819	−6.331	3.512	6.331	2.819	1.756	−4.575	0.284	4.575	4.959
$Fe(F1)_2$	−2.338	−4.300	1.962	4.300	2.338	0.981	−3.319	0.510	3.319	5.615
$Cu(F1)_2$	−2.507	−4.341	1.834	4.341	2.507	0.917	−3.424	0.545	3.424	6.392
$VO(F2)_2$	−3.057	−5.214	2.157	5.214	3.057	1.079	−4.136	0.464	4.136	7.929
$Ni(F2)_2$	−3.255	−5.170	1.915	5.170	3.255	0.958	−4.213	0.522	4.213	9.266
Gallic acid	−1.630	−6.440	4.840	6.440	1.630	2.400	−4.030	1.340	4.030	3.390
Ascorbic acid	−1.160	−6.710	5.550	6.710	1.160	2.540	−4.170	1.130	4.170	3.420
Indomethacin	−2.160	−6.000	3.840	6.000	2.160	1.920	−4.080	1.560	4.080	4.330

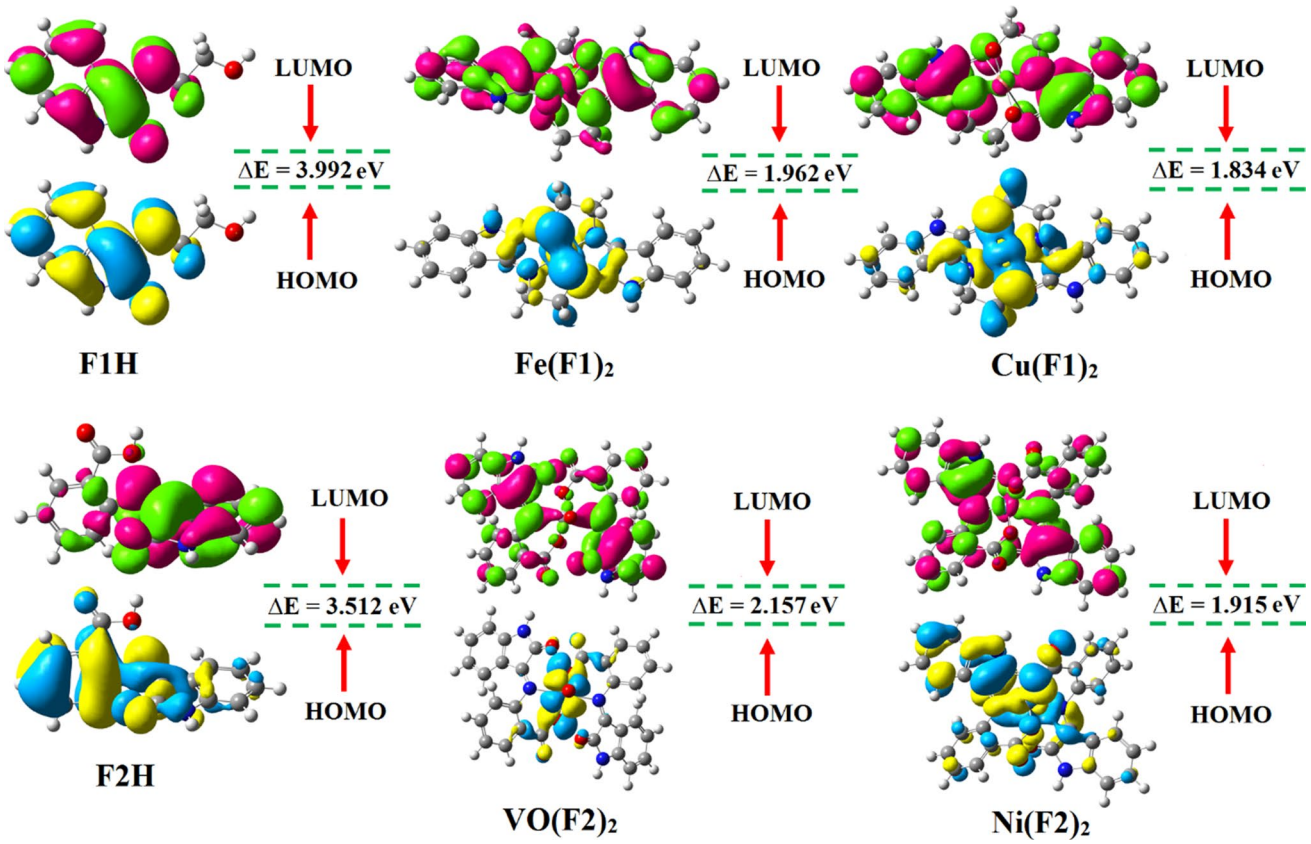

Fig. 2 Frontier molecular orbitals of ligands **(F1H)** and **(F2H)** [color codes for orbitals; yellow (positive) and blue (negative) in HOMO, while pink (positive) and green (negative) in LUMO]

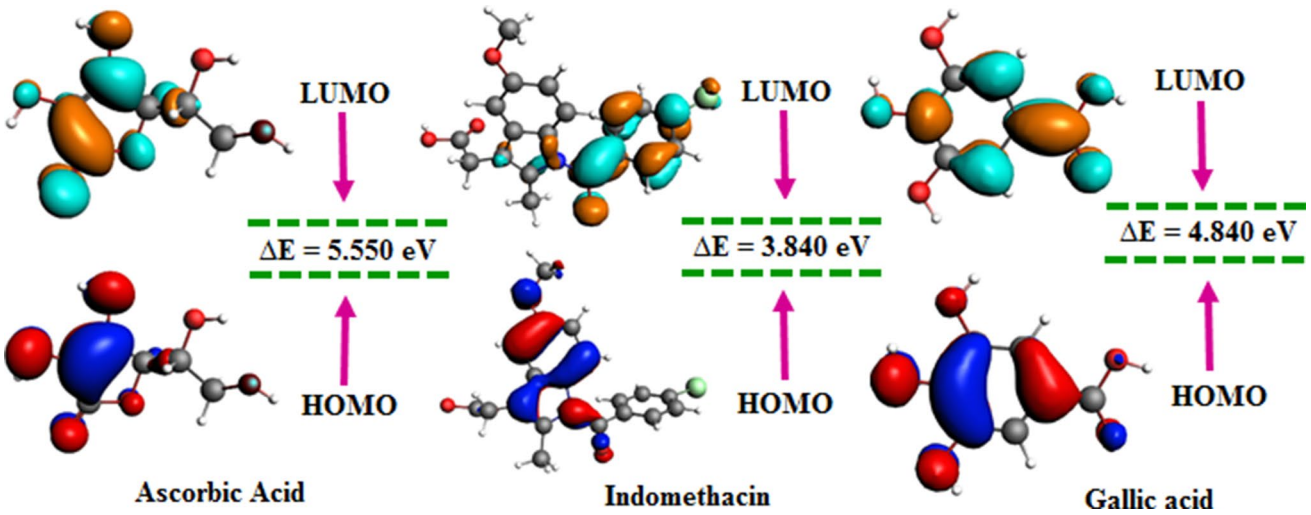

Fig. 3 Frontier molecular orbitals of standard compounds [color codes for orbitals; red and orange colors illustrate the positive, while both blue colors illustrate the negative part of orbitals]

Frontier molecular orbital (FMO) analysis

Frontier molecular orbitals are used to explore and describe the optical parameters, stability, chemical reactivity and electrical parameters. HOMO and LUMO act as donor and acceptor, and electron excitation occurs from HOMO to LUMO. In this study, the FMOs energies, *i.e.*, E_{HOMO}, E_{LUMO}, and their energy gaps $\Delta E_{HOMO-LUMO}$ΔH–L were quantified by the use of B3LYP/6–311 + + G(d,p) for both isatin-derived ligands, their selective metal complexes as well as reference compounds (ascorbic acid, indomethacin and gallic acid) (Hassan et al. 2021) as depicted in Table 2 and displayed in Fig. 2 and Fig. 3. The antimicrobial action and antioxidant aptitude of compounds are strongly associated with the spatial distribution of occupied molecular orbitals signifying most appropriate sites in investigated compounds that are susceptible for attack by reactive agents besides free radicals. The overlapped FMOs indicated extremely responsive behavior of the studied compounds concerning the antioxidant and antimicrobial action.

The DFT data revealed that ligands **(F1H)** and **(F2H)** contain 366 and 497 molecular orbitals, out of which orbital numbers 50, 69, and 51, 70 acts as HOMO and LUMO, correspondingly. For ligands **(F1H)** and **(F2H)**, the energies of HOMO and LUMO were found to be − 6.540, − 6.331 and − 2.548, − 2.819 eV, respectively. The energy gaps of the above said orbitals were obtained to be 3.992 and 3.512 eV, respectively, for both ligands. The descending order of E_{LUMO} for all the studied compounds was found as: **Ni(F2)$_2$** (− 3.255) > **VO(F2)$_2$** (− 3.057) > **(F2H)** (− 2.819) > **(F1H)** (− 2.548) > **Cu(F1)$_2$** (− 2.507) > **Fe(F1)$_2$** (− 2.338) > **indomethacin** (− 2.160) > **gallic acid** (− 1.630) > **ascorbic acid** (− 1.160). The opposite trend for E_{HOMO} was observed as; **ascorbic acid** (− 6.710) > **(F1H)** (− 6.540) > **gallic acid** (− 6.440) > **(F2H)** (− 6.331) > **indomethacin** (− 6.000) > **VO(F2)$_2$** (− 5.214) > **Ni(F2)$_2$** (− 5.170) > **Cu(F1)$_2$** (− 4.341) > **Fe(F1)$_2$** (− 4.300). The susceptibility in the $\Delta E_{HOMO-LUMO}$ was noted as: **ascorbic acid** (5.550) > **gallic acid** (4.840) > **(F1H)** (3.992) > **indomethacin** (3.840) > **(F2H)** (3.512) > **VO(F2)$_2$** (2.157) > **Fe(F1)$_2$** (1.962) > **Ni(F2)$_2$** (1.951) > **Cu(F1)$_2$** (1.834).

In the HOMO and LUMO of ligand **(F1H)**, the electronic charge was accumulated over the whole structure of ligand, *3-[(2-hydroxyethyl)imino]-1,3-dihydro-2H-indol-2-one* with the exception of methylene (CH_2) and hydroxyl (OH) groups, while in the HOMO of ligand **(F2H)**, the electronic charge density was partially distributed on the entire structure of ligand, *2-{[2-oxo-1,2-dihydro-3H-indol-3-ylidene] amino}benzoicacid*. But in the LUMO of ligand **(F2H)**, the charge density was only focused on the azomethine linkage and anthranilic acid part of the ligand. Likewise, in HOMO of **Fe(F1)$_2$** and **VO(F2)$_2$**, the charge density was concentrated on the respective metal centers and the coordinating groups, while in the HOMO of **Cu(F1)$_2$** and **Ni(F2)$_2$**, the charge density was spared over the whole structure but mostly on the respective metal centers and the coordinating groups. Moreover, in LUMO of metal complexes, electronic charge density was scattered on the entire structures.

Global reactivity descriptors

The density functional theory (DFT) is effective in quantifying numerous quantum chemical reactivity descriptors, which are utilized to evaluate the chemical reactivity besides the reactive site peculiarity of chemical systems.

The FMO band energies were used to calculate global reactivity descriptors (as shown in equations S1–S6), which gave information about the behavior of the studied compounds such as stability, reactivity and softness–hardness as shown in Table 2 (Sumrra et al. 2021a, b, c). The decreasing order of IP was found as **ascorbic acid** (6.710) > **(F1H)** (6.540) > **gallic acid** (6.440) > **(F2H)** (6.331) > **indomethacin** (6.000) > **VO(F2)$_2$** (5.214) > **Ni(F2)$_2$** (5.170) > **Cu(F1)$_2$** (4.341) > **Fe(F1)$_2$** (4.300). While the EA order was: **Ni(F2)$_2$** (3.255) > **VO(F2)$_2$** (3.057) > **(F2H)** (2.819) > **(F1H)** (2.548) > **Cu(F1)$_2$** (2.507) > **indomethacin** (2.160) > **gallic acid** (1.630) > **ascorbic acid** (1.160).

Among the studied ligands, **(F1H)** contained the greatest IP value as 6.540 eV, whereas **(F2H)** exhibited the lowest value as 6.331 eV. Similarly, **(F2H)** possessed maximum EA value, 2.819 eV; however, **(F1H)** exhibited minimum EA value, 2.548 eV. Therefore, the electron-donating and accepting behaviors of our ligands **(F1H)** and **(F2H)** were measured by their IP and EA amplitudes, which are actually linked to HOMO–LUMO energy gap [ΔE(eV)]. As a result, the values of IP were found to be greater in magnitude than the EA, signifying that ligands **(F1H)** and **(F2H)** contained good electron-losing potential.

The decreasing order for chemical potential was: **(F2H)** (−4.575) > **(F1H)** (−4.544) > **Ni(F2)$_2$** (−4.213) > **ascorbic acid** (−4.170) > **VO(F2)$_2$** (−4.136) > **indomethacin** (−4.080) > **gallic acid** (−4.030) > **Cu(F1)$_2$** (−3.424) > **Fe(F1)$_2$** (−3.319). Any molecule having smaller value of chemical potential was preferred as a less stable and more reactive molecule and vice versa. The chemical potential for examined ligands **(F1H)** and **(F2H)** was observed to be greater than the other studied compounds. The electronegativity order follows the same trend: **(F2H)** (4.575) > **(F1H)** (4.544) > **Ni(F2)$_2$** (4.213) **ascorbic acid** (4.170) > **VO(F2)$_2$** (4.136) > **indomethacin** (4.080) > **gallic acid** (4.030) > **Cu(F1)$_2$** (3.424) > **Fe(F1)$_2$** (3.319). Among the studied ligands, **(F2H)** has higher electronegativity value (4.575) (Table 2). The obtained data have shown that both the ligands **(F1H)** and **(F2H)** could be considered as chemically hard molecules with strong electron-donating ability besides maximal kinetic stability.

The subsequent descending order of hardness was obtained as: **ascorbic acid** (2.540) > **gallic acid** (2.400) > **(F1H)** (1.996) > **indomethacin** (1.920) > **(F2H)** (1.756) > **VO(F2)$_2$** (1.079) > **Fe(F1)$_2$** (0.981) > **Ni(F2)$_2$** (0.958) > **Cu(F1)$_2$** (0.917), whereas the softness decreased in the following order: **indomethacin** (1.560) > **gallic acid** (1.340) > **ascorbic acid** (1.130) > > **Cu(F1)$_2$** (0.545) > **Ni(F2)$_2$** (0.522) > **Fe(F1)$_2$** (0.510) > **VO(F2)$_2$** (0.464) > **(F2H)** (0.284) > **(F1H)** (0.250). Any chemical system with small ΔE value was considered as reactive, soft and unstable. For the investigated compounds, calculated values of global softness (σ) were smaller in contrast to the global hardness (η); thus, the synthesized isatin-derived compounds were relatively stable and unreactive.

The order of hardness and FMO energy gap was found notably similar and can be summarized as **(F1H)** > **(F2H)** > **VO(F2)$_2$** > **Fe(F1)$_2$** > **Ni(F2)$_2$** > **Cu(F1)$_2$**. The trend for electrophilicity index was: **Ni(F2)$_2$** (9.266) > **VO(F2)$_2$** (7.929) > **Cu(F1)$_2$** (6.392) > **(F2H)** (5.959) > **Fe(F1)$_2$** (5.615) > **(F1H)** (5.170) > **indomethacin** (4.330) > **ascorbic acid** (3.420) > **gallic acid** (3.390). The compounds with minimum values of E_{HOMO} exhibited reduced electron-contributing aptitude, demonstrating that the studied metal complexes might possess superior electron-donating capability in comparison with ligands and some standard compounds. These outcomes came to end with the conclusion that the metal complexes would be better biological active and antioxidant contenders.

Molecular electrostatic potential (MEP) analysis

A molecular electrostatic potential (MEP) plot is utilized to conceptualize different charge distributions in compounds. MEP is basically the interpretation of the three-dimensional electron charge density through graphical interpretation. And by using this 3D MEP plot, the physical and chemical characteristic features of a molecule can be discussed. MEP plot consists of various standard colors: orange, red, blue, yellow and green, indicating the level of electrostatic potential. The descending order for the level of electrostatic potential was: blue > green > yellow > orange > red. MEP analysis helps to recognize negative, positive and neutral zones of the investigated molecules by different shadings. On the MEP map, red color shows a highest negative potential which is actually electron-rich area and considered as a fitting spot for attack by electrophilic species, yellow color also specifies a slightly electron-rich area, and blue indicates a highly positive potential which is basically an electron-deficient zone and could be a better fitting spot for attack by a nucleophilic species. The light blue represents a slightly electron-deficient zone, whereas the green color signifies a neutral zone (Mermer et al. 2020).

In this study, the MEP surfaces of investigated compounds were figured at the B3LYP functional with 6–311 + + G(d,p) level of theory and the pictographic display is presented in Fig. 4, which gives the valuable evidence about the possible electrophilic and nucleophilic sites within the compounds. It could be seen from the MEP surfaces that the red color displaying the electron-rich zone was displayed on the oxygen atoms. Therefore, the possibility of electrophilic attack is maximum at these sites. Blue and green zones were spread over the hydrogen and some carbon atoms specifying the

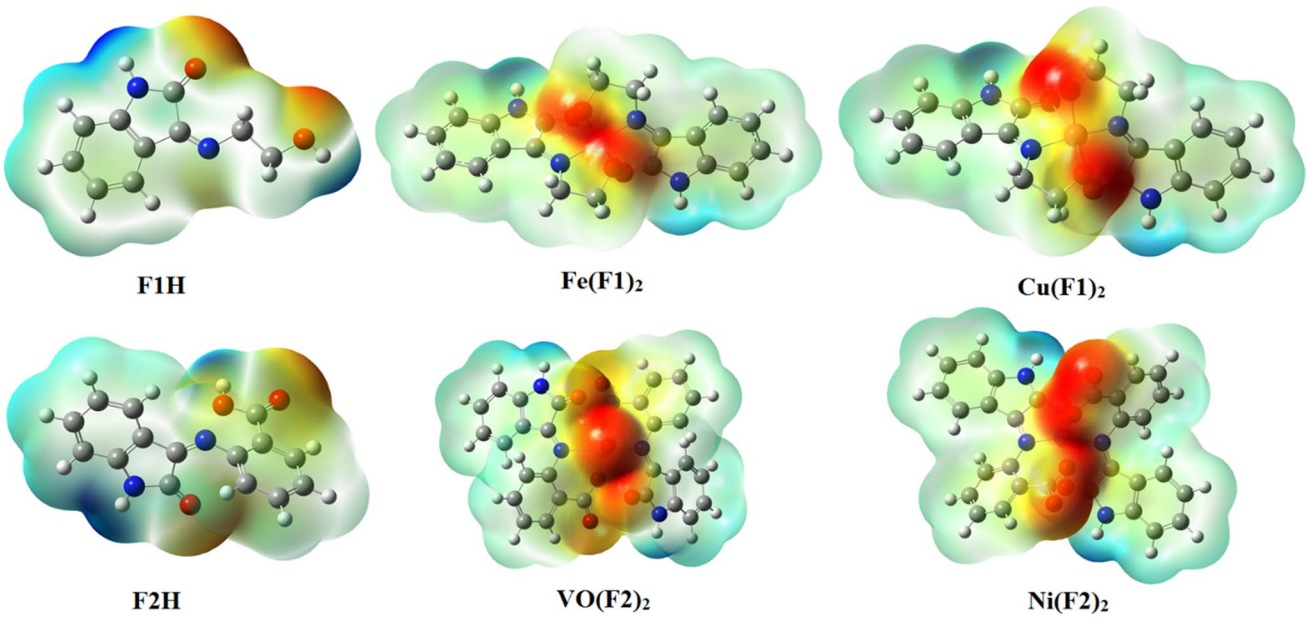

Fig. 4 MEP maps for isatin-derived compounds

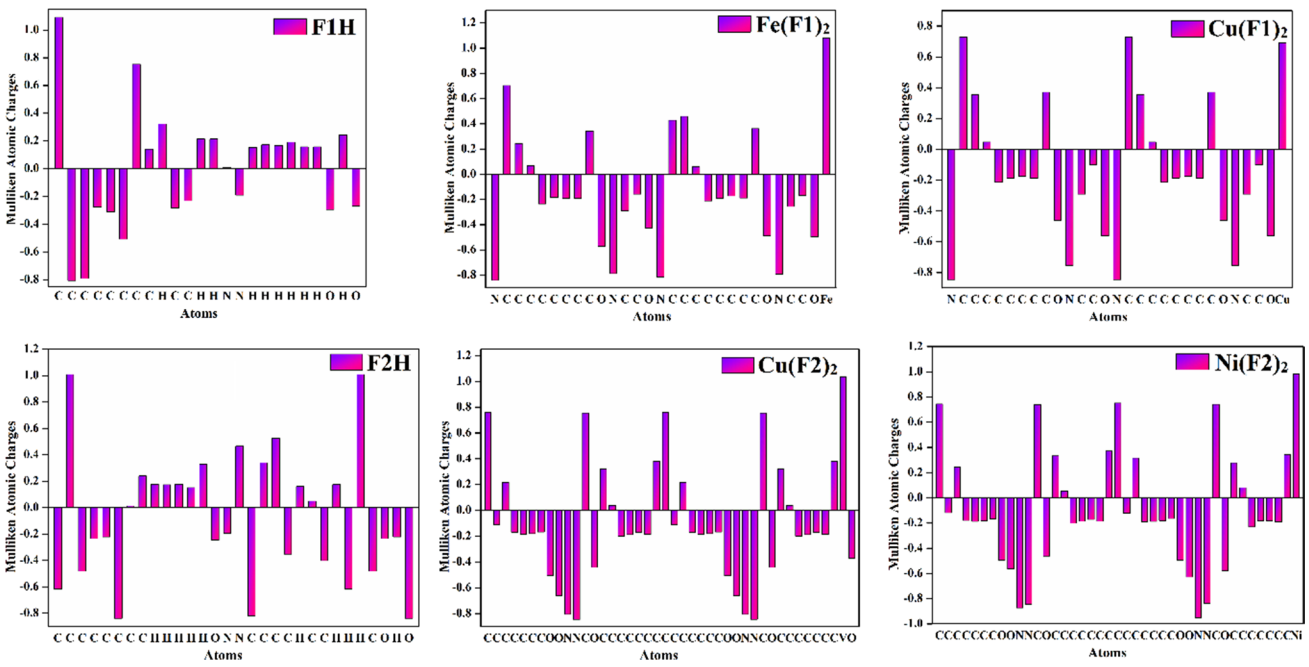

Fig. 5 Histogram of Mulliken atomic charges for isatin-based compounds

electron-deficient zone areas and are implied as the best sites for the encounter of nucleophilic attack. From red, blue and green colors, it is evident that sites for various reactions were present in all the investigated compounds.

Mulliken atomic charges (MAC) analysis

Mulliken population analysis has a very important part in the quantum chemical operation to molecular framework because atomic charges largely affect the electronic structure, polarizability and properties of molecules (Al-Amiery et al. 2012). Mulliken atomic charges for isatin-derived ligands and their selected metal complexes were computed through B3LYP/6–311 + + G(d,p) and are given in Tables S3 and S4. Mulliken atomic charges were also represented as histograms in Fig. 5. The optimized structures of both ligands with atoms involved in these histograms are shown in Fig. 1. The Mulliken atomic charges showed the existence of greater electronegative atoms: N15 = − 0.191, O22 = − 0.295 and O24 = − 0.269 for ligand **(F1H)**, while O14 = − 0.246, N15 = − 0.197, O28 = − 0.235 and O30 = − 0.839 for ligand **(F2H)**, which has positive charge distribution on carbon atoms, while all hydrogen atoms carry positive charge (as shown in Fig. S10).

The MAC data of metal complexes have also shown unequal redistribution of the electronic charge density over the benzene rings due to the presence of atoms with high electronegativity in the structure such as nitrogen and oxygen. On the other hand, metals of the studied complexes **$Fe(F1)_2$, $Cu(F1)_2$, $VO(F2)_2$** and **$Ni(F2)_2$** were found to have greater electropositive values of Fe29 = 1.078, Cu29 = 0.692, V41 = 1.036 and Ni41 = 0.984, respectively.

Natural bond orbital (NBO) analysis

NBO analysis is a very excellent tool to analyze the interactions in a molecular framework. The stabilization energy obtained through this analysis directly affects the hyperconjugative associations between donors and acceptors. NBO analysis was performed to compare and analyze the coordinating capability of ligands. NBO analysis provides an explanation of the molecular structure by a set of two center localized antibonding and bonding orbitals along with valence lone pair and one center core pair orbital. The analysis is established on the second-order perturbation theory concerned with the Fock matrix. The findings of NBO analysis were used to study and explore the second-order interactions between lone pair (LP) orbitals and empty anti-bonding orbitals (σ* or π^*) as a measure for probable coordination ability and localization of lone pair (Weinhold et al. 2016).

The NBO calculations for isatin-based ligands and their selective metal complexes were measured at DFT/B3LYP/6–311 + + G(d,p) method to obtain the perturbation theory. Very large data were obtained through analysis, but here only promising transitions which have a greater value of stabilization energies are shown in Table S5. The optimized structures of studied compounds with numbering are shown in Fig. 1. For ligand **(F1H)**, the transfer of charge from $\pi(C_2-C_3) \rightarrow \pi^*(C_1-C_6)$, $\pi(C_8-O_{24}) \rightarrow \pi^*(C_7-N_{14})$ leads to the stabilization energies as 251.32 and 62.29 kJmol^{-1}, respectively, that showed strong delocalization within the system. For ligand **(F2H)**, the charge transfer from $\pi(C_1-C_6) \rightarrow \pi^*(C_2-C_3)$, $\pi(C_{17}-C_{19}) \rightarrow \pi^*(C_{18}-C_{20})$ and $\pi(C_{17}-C_{19}) \rightarrow \pi^*(C_{22}-C_{23})$ leads to the stabilization energies as 355.00, 288.62 and 208.60 kJmol^{-1}, respectively, that showed strong delocalization within the system.

The interactions of lone pairs (LPs) of nitrogen and oxygen with different antibonding orbitals were considered in both ligands. All the LPs mainly have p character, and they are practically filled with two electrons. The interaction of LPs with antibonding orbitals results in the donation of electrons from LPs to antibonding orbitals. The stabilization energy $E^{(2)}$ related to these interactions could be utilized as a measure of the involvement of the lone pairs in the intramolecular delocalization.

The greater stabilization energy value results in highly intensive interaction between electron-donating LPs and electron-accepting antibonding orbitals (Srivastava and Misra 2014). The LP of N_{14} and N_{15}, interacted with antibonding orbitals, lone pair (1) $N_{14} \rightarrow \sigma^*(C_7-C_8)$, $N_{15} \rightarrow \pi^*(C_2-C_3)$ and $N_{15} \rightarrow \pi^*(C_8-O_{24})$ resulted in significant stabilization by 15.94, 36.78 and 54.40 kJmol^{-1}, respectively, in ligand **(F1H)**, while the LP of N_{15} and N_{16}, interacted with antibonding orbitals, lone pair (1) $N_{16} \rightarrow \sigma^*(C_7-C_8)$, $N_{16} \rightarrow \pi^*(C_{17}-C_{19})$, $N_{15} \rightarrow \pi^*(C_1-C_6)$ and $N_{15} \rightarrow \pi^*(C_7-O_{14})$ gave rise to enormous stabilization by 19.10, 21.26, 43.12 and 65.05 kJmol^{-1}, respectively, in ligand **(F2H)**.

In comparison, the interactions of the second lone pair of oxygen contributed less amount of stabilization (less than half of that of nitrogen). The LP of O_{24} interacted with antibonding orbitals, lone pair (2) $O_{24} \rightarrow \sigma^*(C_7-C_8)$ and $O_{24} \rightarrow \sigma^*(C_8-N_{15})$ caused substantial stabilization by 21.50 and 26.76 kJmol^{-1}, respectively, signifying the strong conjugative interaction of O to C–C, C–N and C–O in ligand **(F1H)**. The LP of O_{14}, O_{28} and O_{30} interacted with antibonding orbitals, lone pair (2) $O_{30} \rightarrow \sigma^*(C_{19}-C_{27})$, $O_{14} \rightarrow \sigma^*(C_7-C_8)$, $O_{14} \rightarrow \sigma^*(C_7-N_{15})$, $O_{30} \rightarrow \sigma^*(C_{27}-C_{28})$ and $O_{28} \rightarrow \pi^*(C_{27}-C_{30})$ resulted in significant stabilization by 20.20, 26.47, 32.52, 38.54 and 51.16 kJmol^{-1}, respectively,

specifying the strong conjugative interaction of O to C–C, C–N and C–O in ligand **(F2H)**. In both ligands **(F1H)** and **(F2H)**, the main p character of N(1) lone pair orbitals along with little participation in the intramolecular hyperconjugation exhibits behavior relevant to pure LP orbitals.

Therefore, on the basis of the results of NBO analysis, it can be established that nitrogen atoms of azomethine [N_{14} in **(F1H)** and N_{16} in **(F2H)**] are more reactive and have the maximum ability to coordinate with metal ions than oxygen atoms. Thus, the reduced energy involved in the hyper-conjugative interactions of lone pair of nitrogen suggested that it has a comparatively greater coordination tendency. Similarly, the $\pi \rightarrow \pi^*$ interactions such as $\pi(C_{18}-C_{19}) \rightarrow \pi^*(C_{17}-N_{25})$, $\pi(C_4-C_5) \rightarrow \pi^*(C_3-N_{11})$, $\pi(C_{35}-C_{36}) \rightarrow \pi^*(N_{30}-C_{34})$ and $\pi(C_{34}-C_{35}) \rightarrow \pi^*(N_{30}-Ni_{41})$ yielded 27.15, 11.65, 12.52 and 43.39 kJmol^{-1} stabilization energies for complexes **Fe(F1)$_2$, Cu(F1)$_2$, VO(F2)$_2$** and **Ni(F2)$_2$**, respectively. Moreover, the LP $\rightarrow \pi^*$ interactions were seen as $N_1 \rightarrow \pi^*(C_8-C_9)$, $N_1 \rightarrow \pi^*(C_2-C_{10})$, $N_{11} \rightarrow \pi^*(C_{12}-C_{13})$ and $N_{11} \rightarrow \pi^*(N_{30}-Ni_{41})$ afforded stabilization energies of 37.63, 29.88, 29.15 and 62.47 for complexes **Fe(F1)$_2$, Cu(F1)$_2$, VO(F2)$_2$** and **Ni(F2)$_2$**, correspondingly. This NBO analysis showed strong interactions, stabilization energies, coordination tendency and stability of studied compounds.

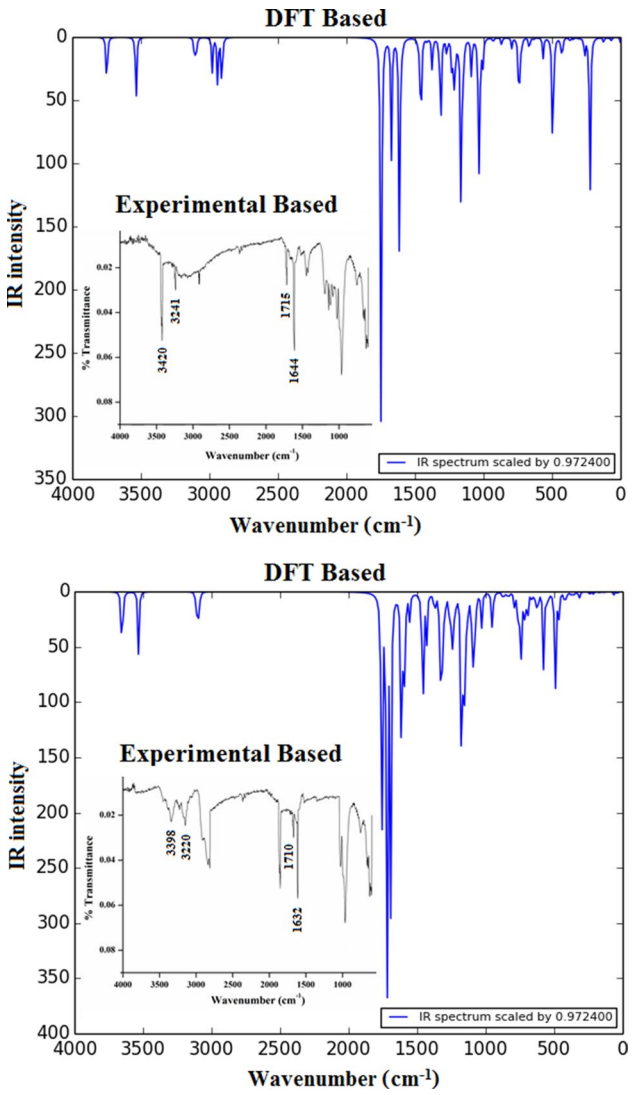

Fig. 6 Experimental and computed vibrational spectra of ligands **(F1H)** and **(F2H)** with the broadening parameter of 10 cm^{-1}

Computational IR analysis

The experimental IR spectra of both ligands and their respective metal complexes were also compared with theoretical computed data, and results showed a close agreement between both values. The experimental and computed data of ligands are given in Tables S6 and S7, along with their intensities and vibrational assignments. The vibrational frequencies were calculated at DFT/B3LYP with 6–311 + + G(d,p) basis set, as illustrated in Fig. 6 for ligands and in Fig. S11 for complexes. Generally, the computed vibrational frequencies by DFT are obtained slightly higher than the experimental ones, which have been improved by using a scale factor of 0.9724 (Altürk et al. 2017). Infrared (IR) spectroscopy has been acknowledged as an effective approach in the hydrogen-bond research (Issaoui et al. 2009; Rekik et al. 2007a). Vibrational properties and frequencies are strongly affected by hydrogen-bond interactions (Rekik et al. 2007b). A redshift in the stretching vibrations, band broadening and increase in intensity of C–O and OH vibrations are considered as the most common consequences of hydrogen bonding (Issaoui et al. 2010).

C–H vibrations: The C–H stretching vibrations were easily predicted through DFT frequencies and are generally fall in the 3000–3100 cm^{-1} range of IR spectra (Prabavathi et al. 2014). The experimental C–H stretching frequencies of both ligands appeared at 3110–3191 cm^{-1} range, which agreed well with the theoretical frequencies obtained at 3022–3198 cm^{-1}. The vibrations of C–H (bending) are generally observed in the 1000–1300 cm^{-1} range (Arivazhagan et al. 2015). The computed values (1039–1303 cm^{-}) well support experimental values found at 1052–1325 cm^{-1}. For ligand **(F1H)**, the C–H aliphatic bands were observed experimentally at 2917 and 2989 cm^{-1} which are well agreed with the theoretical values at 2991 and 3022 cm^{-1}. The small variation in the experimental and computed frequencies is may be due to solid-state interactions of ligands for spectral studies, but no interactions for gaseous sample utilized for computational studies.

Ring vibrations: The stretching ring vibrations are normally observed at 1400–1650 cm^{-1}. The theoretical frequencies observed at 1513 and 1598 cm^{-1} showed a close agreement to the experimental values at 1563 and 1625 cm^{-1}

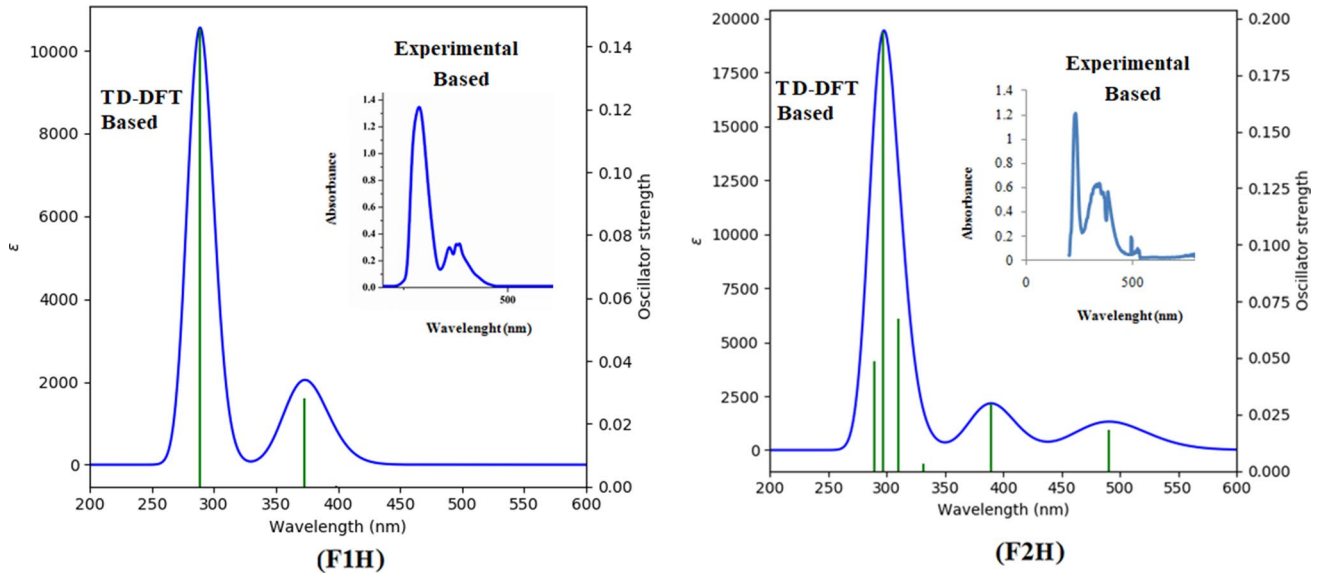

Fig. 7 Experimental and calculated electronic spectra of ligands **(F1H)** and **(F2H)** with the broadening parameter of 2000 cm^{-1} for **(F1H)** and 3000 cm^{-1} for **(F2H)**

Table 3 Antibacterial and antifungal activity of ligands and their metal chelates

Compounds	Antibacterial Activity, Zone of Inhibitions/mm				Antifungal Activity, Zone of Inhibitions/mm		
	A	B	C	D	E	F	G
(F1H)	00	13	31	19	08	00	15
(F2H)	20	22	27	00	17	00	00
$VO(F1)_2$	13	21	20	07	14	00	19
$Fe(F1)_2$	00	16	16	00	19	10	20
$Co(F1)_2$	00	30	29	22	24	11	24
$Ni(F1)_2$	07	21	24	00	30	20	30
$Cu(F1)_2$	06	20	23	11	21	18	31
$Zn(F1)_2$	17	30	22	10	00	16	00
$VO(F2)_2$	23	26	21	12	11	11	07
$Fe(F2)_2$	21	21	20	16	09	20	00
$Co(F2)_2$	26	18	19	10	00	20	00
$Ni(F2)_2$	30	21	21	18	21	29	00
$Cu(F2)_2$	24	32	26	25	23	23	00
$Zn(F2)_2$	00	21	13	23	20	20	30
SD	38	40	35	33	34	37	42

A = *Escherichia coli*, B = *Staphylococcus aureus*, C = *Pseudomonas syringae*, D = *Streptococcus pyogenes*, E = *Aspergillus niger*, F = *Rhizopus stolonifer*, G = *Trichoderma spirale*, SD = Standard Drug (Amoxicillin for antibacterial activity, Fungom for antifungal activity)

as weak bands indicating carbon–carbon single and double bonds.

N–H vibrations: These vibrations for ligands **(F1H)** and **(F2H)** were observed at 3241 and 3220 cm^{-1}, respectively, while the computed frequencies were found at 3634 and 3635 cm^{-1}. This difference in computed and experimental values may be attributed to the presence of solid-state intermolecular interactions in the compounds during the spectral study, while such interactions are ignored for the sample by considering it as a single molecule in the gas phase used for computational studies.

C = O vibrations: The experimental C = O stretching vibrations were observed at 1709–1715 cm^{-1} for both ligands, which are consistent with the computed frequencies at 1769–1795 cm^{-1}.

Computational UV–Vis analysis

The TD spectra for isatin Schiff base ligands and their selected metal complexes were carried out through TD-DFT in the gas phase. For ligand **(F1H)**, the computed spectral analysis showed bands $\pi \rightarrow \pi^*$ and $n \rightarrow \pi^*$ electronic transitions at 402, 375, 289, 277, 262 and 235 nm, which agreed well with the experimentally observed peaks at 400 and 289 nm, as given in Fig. 7. Similarly, for ligands **(F2H)**, the computed spectra showed $\pi \rightarrow \pi^*$ and $n \rightarrow \pi^*$ electronic transitions at 490, 389, 331, 310, 297 and 289 nm, which were found to be in good agreement with the experimentally observed peak values at 490, 400 and 250 nm. These intra-ligand transitions are commonly attributable to the presence of (C = C), (C = O) and (C = N) groups in the structures of both ligands.

The theoretical and experimental wavelengths, excitation energies, oscillator strengths and atomic orbital contributions of ligands and their selected metal complexes are given in Tables S8 and S9, whereas the theoretical spectra of complexes are shown in Fig. S12. The computed data also showed some other transitions which can be considered as forbidden because their oscillator strengths are almost zero. Therefore, the DFT-based vibrational modes computed for both isatin-derived ligands and their corresponding complexes were found to be in good rational agreement with the experimental findings.

Antimicrobial activity

Antibacterial activity

Isatin-based ligands and their corresponding transition metal chelates were tested for antibacterial activity against two Gram-positive (*S. pyogenes, S. aureus*) and two Gram-negative (*P. syringae, E. coli*) bacterial strains. The results of antibacterial activity are displayed in Table 3 and Fig. 8 as inhibition zones in millimeters and compared with standard drug amoxicillin. The results revealed that ligand **(F2H)** was inactive against **D** and showed moderate activities for other strains. Similarly, metal complexes also showed good results for antibacterial activity. The complex $\mathbf{Ni(F2)_2}$ showed maximum activity for **A** and moderate activity for **B**, **C** and **D**, while $\mathbf{Cu(F2)_2}$ showed maximum activity, *i.e.,* 32 mm and 25 mm for **B** and **D**, and significant results for **A** and **C** as 24, 26 mm, respectively. All other complexes showed good results, and the increase in the activity of complexes in contrast to ligands was due to the chelation process.

The antibacterial profile of these compounds has been compared with the similar type of isatin-derived Schiff bases, and their resulting metal complexes have already been published in the literature. All the values of inhibition zones were in good agreement with the reported results (Table S10). But in most cases, the compounds have exhibited more antibacterial properties than the published results.

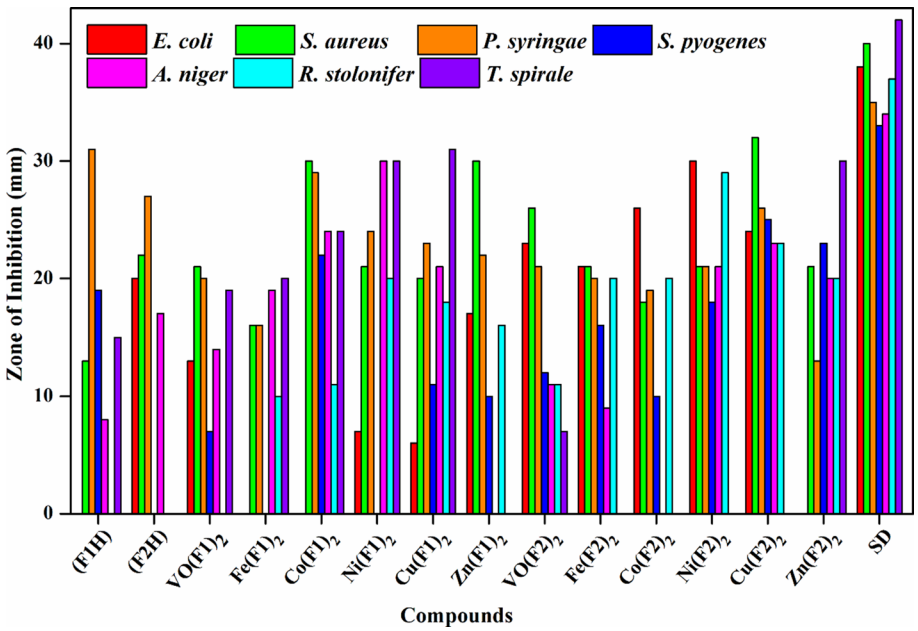

Fig. 8 Antibacterial and antifungal activity of synthesized isatin-based compounds

Antifungal activity

The antifungal activity of metals based isatin ligands was checked using three fungal strains: *A. niger* (**E**), *R. stolonifer* (**F**) and *T. spirale* (**G**). The results were recorded as inhibition zones in millimeters as shown in Table 3 and Fig. 8. The results were also compared with the reference antifungal drug, Fungom. The results revealed that the ligand **(F1H)** was inactive against **F**, but exhibited reduced activity for **E**. And the ligand **(F2H)** was inactive against two fungal strains **F** and **G**. The complexes $\mathbf{Zn(F1)_2}$ and $\mathbf{Co(F2)_2}$ were inactive against **E**, and $\mathbf{VO(F1)_2}$ was inactive against **F** strain. All the complexes of ligand **(F2H)** were inactive against **G** except complex $\mathbf{Zn(F2)_2}$ that showed significant activity of 30 mm and $\mathbf{VO(F2)_2}$ that showed the least activity of 7 mm. Overall complexes $\mathbf{Ni(F1)_2}$, $\mathbf{Cu(F1)_2}$ and $\mathbf{Zn(F2)_2}$ exhibited significant activity, while the other complexes showed good to moderate activity against all fungal strains. The observed increase in the activity of complexes in contrast to the ligands was due to the chelation process.

The antifungal potential of these compounds has been compared with the similar type of isatin-derived Schiff bases, and their resulting metal complexes have already been published in the literature. All the values of inhibition zones were in good agreement with the reported results (Table S10). But in most cases, the compounds have exhibited more fungicidal properties than the published results.

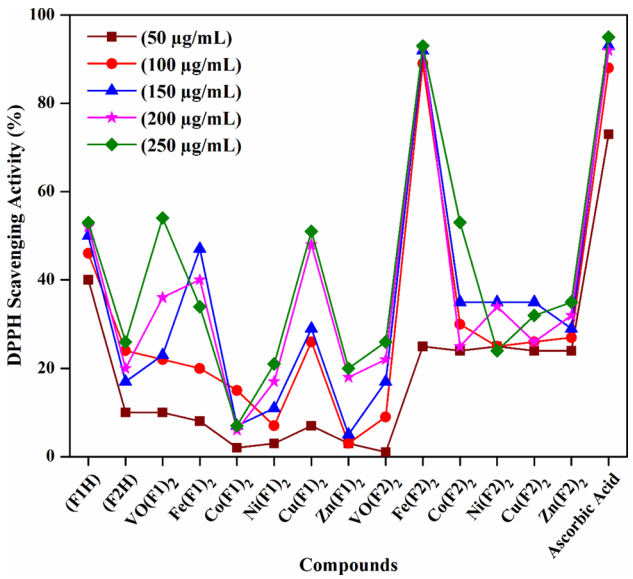

Fig. 9 Antioxidant activity of synthesized isatin-based compounds

Antioxidant activity

Antioxidant activity of metals based isatin ligand was checked by DPPH radical scavenging assay and phosphomolybdate assay.

DPPH assay

The diphenylpicrylhydrazide (DPPH) is stable and free radical, which was utilized to determine the radical scavenging activity of isatin-based ligands and their derived metal complexes. Different concentrations (*i.e.,* 50, 100, 150, 200 and 250 µg/mL) of as-synthesized compounds and ascorbic acid (standard) were used for this activity, and absorbance was measured at 517 nm. After that, the inhibition results of synthesized compounds were compared with ascorbic acid. The results also showed that percentage inhibition was increased by increasing the concentration of compounds, as

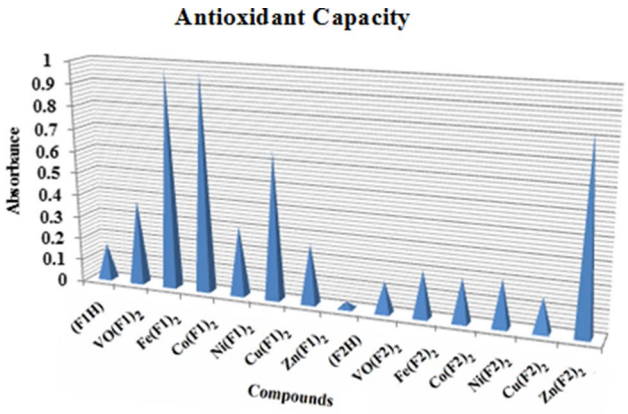

Fig. 10 Total antioxidant capacity of synthesized isatin-based compounds

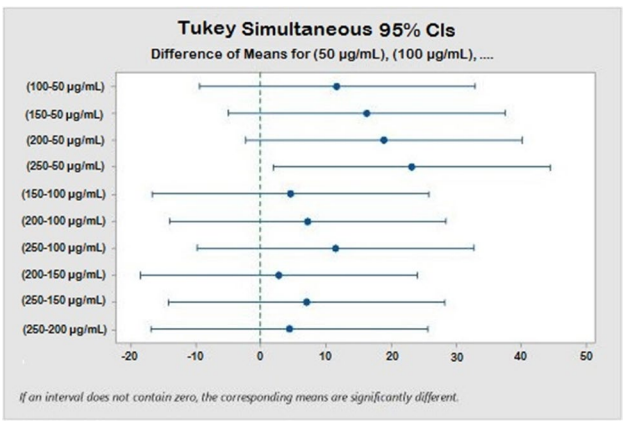

Fig. 11 Tukey plot for 50, 100, 150, 200 and 250 µg/mL

shown in Fig. 9 and Table S11. The results revealed weak to moderate activity for synthesized ligands and complexes. Ascorbic acid has shown maximum DPPH scavenging activity. Among the synthesized compounds, highest activity was shown by **Fe(F2)$_2$** complex, *i.e.,* 93%. Cobalt complex **Co(F2)$_2$** also showed well activity, *i.e.,* 53%.

Phosphomolybdate assay

The total antioxidant capacity of compounds was evaluated using a phosphomolybdate assay. In this method, a reagent solution (obtained by mixing sodium phosphate (0.028 M), ammonium heptamolybdate (0.04 M) and sulfuric acid (5 mL) was used and measured absorbance at 695 nm. The results revealed that **VO(F2)$_2$** complex showed the highest absorbance, *i.e.,* 0.8376. The results also revealed that most of metal complexes showed higher absorbance than their parent ligand, as shown in Table S12 and Fig. 10.

Statistical analysis

One-way analysis of variance (ANOVA) is a statistical and advanced research method that is concerned with comparing means of different samples. It was used to interpret the experimental outcomes of biological activities for all the prepared compounds and to see the significant difference in the performance of all treatments. Furthermore, multiple comparison test, particularly Tukey's test, was used to determine the most significant treatment effect among all compounds. For antibacterial activity, the results obtained through ANOVA and Tukey test showed that performance of B has a highly significant effect as compared to other strains A, C and D as shown in Table S13.

Similarly, for antifungal activity the results showed that no treatment has significant effect because for all **E**, **F** and **G** strains the p-value is greater than 0.05 as shown in Table S14. For antioxidant activity, the results showed that performance of 50 µg/mL and 250 µg/mL has significant effect than all other concentrations as shown in the table of Tukey pairwise comparison the p-value for this is 0.02 which is less than 0.05. The graphs of interval plots and Tukey test are shown in Figs. 11 and S13–S17.

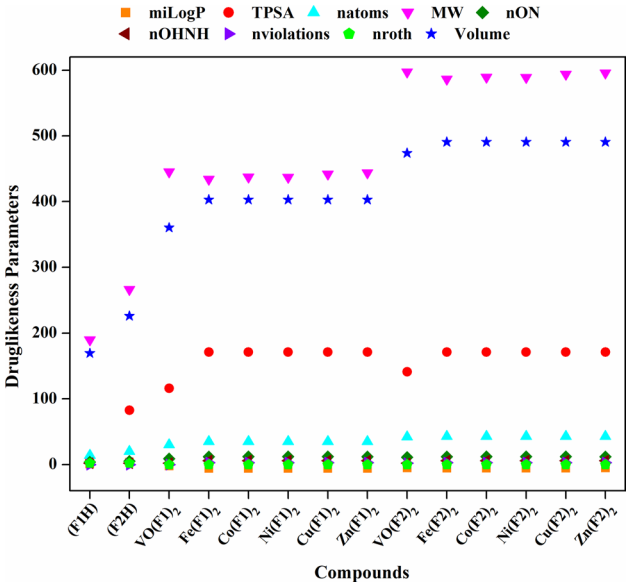

Fig. 12 Drug-like properties of the synthesized ligands **(F1H)** and **(F2H)** and their respective metal complexes determined by the Lipinski law

Table 4 Drug-likeness properties of synthetic compounds by Lipinski's rule

Synthetic Compounds	Drug−likeness Parameters								
	miLogP	TPSA	natoms	MW	nON	nOHNH	nviolations	nroth	Volume
(F1H)	0.91	5.45	14	190.19	4	2	0	2	169.47
(F2H)	3.28	82.53	20	266.25	5	2	0	2	226.26
$VO(F1)_2$	−2.27	115.95	30	445.32	9	2	0	0	360.25
$Fe(F1)_2$	−6.04	171.10	35	434.22	12	6	3	0	402.75
$Co(F1)_2$	−5.94	171.10	35	437.31	12	6	3	0	402.75
$Ni(F1)_2$	−5.94	171.10	35	437.07	12	6	3	0	402.75
$Cu(F1)_2$	−6.02	171.10	35	441.92	12	6	3	0	402.75
$Zn(F1)_2$	−5.89	171.10	35	443.79	12	6	3	0	402.75
$VO(F2)_2$	−5.17	141.41	42	597.43	11	2	2	0	473.82
$Fe(F2)_2$	−5.56	171.10	43	586.33	12	6	3	0	490.73
$Co(F2)_2$	−5.41	171.10	43	589.42	12	6	3	0	490.73
$Ni(F2)_2$	−5.41	171.10	43	589.18	12	6	3	0	490.73
$Cu(F2)_2$	−5.50	171.10	43	594.03	12	6	3	0	490.73
$Zn(F2)_2$	−5.33	171.10	43	595.87	12	6	3	0	490.73

Drug-likeness analysis

In silico drug-likeness assessment involves the detailed examination of the structural and physiochemical features of the compounds to order to determine their potential to develop as an oral drug-like candidate. To determine whether the lipophilicity and biocompatibility of the compounds are associated with synthetic compounds, computational engine called Molinspiration (version 2018.10) has been used to evaluate and present physiochemical properties as depicted in Table 4 (Noreen and Sumrra 2021). The octanol–water partition coefficient (miLogP) for both ligands **(F1H)** and **(F2H)** was less than five (0.91–3.28), signifying a stronger permeability, higher mobility and a more soluble character all over the cell membrane (Fig. 12). All the metal complexes have negative value of miLogP ranging from − 2.27 to − 6.04, that signified their high affinity having strong interactive process with the targeted proteins. The lower values of miLogP have displayed that these compounds have ability to bind with targeted proteins. The TPSA (total polar surface area) potentials for these synthetic compounds indicate that when they are used as drugs, they have the ability to dissolve well with the purpose of attaching to a specific purpose. For the studied compounds, TPSA ranges from 5.45 to 171.10. The ligand **(F1H)** exhibited the lowest value of TPSA, while the complexes have shown the highest value of TPSA.

The molecular weight of both the synthesized ligands **(F1H)** and **(F2H)** was less than 500 g/mol, demonstrating their superior ability to move, digest and disperse. All metal complexes, on the other hand, have a higher molecular mass ranging from 434.22 to 597.43 g/mol, which may reduce their readable drug-likeness aptitude (move, digest or disperse) to some extent. In agreement with Lipinski law, hydrogen-bond acceptors (oxygen and nitrogen) along with donor atoms were determined in the accepted range in all hydrogen-bond tests (OH and NH). All the metal complexes were found to have the maximum rotative relations of 3 with regard to Lipinski law. No rotary hydrogen was found for the ligands. The ligands **(F1H)** and **(F2H)** have exhibited less volume as 169.47 and 226.26, respectively, while their metal complexes had greater volume ranging from 360.25 to 490.73.

Conclusion

Assessment of the intrinsic structural modifications inflicted by the coordination of transition metals in the molecular geometries of isatin Schiff base ligands is of primary importance for detailed characterization and thoughtful structure–activity relationships. We made an effort to scrutinize the coordinating aspects of isatin ligands as efficacious metal-binding entities involving a combined synthetic and computational approach. Two new isatin-based ligands, namely *3-[(2-hydroxyethyl)imino]-1,3-dihydro-2H-indol-2-one* **(F1H)** and *2-{[2-oxo-1,2-dihydro-3H-indol-3-ylidene]amino}benzoic acid* **(F2H)**, were synthesized and complexed with divalent and tetravalent 3*d*-metal ions. The synthesis was carried out efficiently using the condensation method, and spectroscopic studies supported the anticipated structures of the isatin compounds. The vibrational frequencies and electronic transitions of the studied compounds have been DFT-computed and then compared with experimental findings. Overall, the DFT findings revealed excellent concurrence with the experimentally observed data, which confirmed the purity of synthesized compounds.

For ligands **(F1H)** and **(F2H),** the FMO energy gap (HOMO–LUMO) was 3.992 eV and 3.512 eV, respectively. The low FMO energy gap revealed the stability of the ligand **(F1H)**. The minimum E_{HOMO} values exhibited reduced electron-contributing aptitude, demonstrating that both ligands **(F1H)** and **(F2H)** might have better electron-donating capability in comparison with other compounds. NBO analysis concluded that nitrogen atoms of azomethine [N_{14} in **(F1H)** and N_{16} in **(F2H)**] are more reactive and able to coordinate with metal ions than oxygen atoms. The synthesized isatin compounds have shown varying degrees of inhibition effects on the growth of tested fungal and bacterial species. Besides the antimicrobial activity, all the compounds have also exhibited a moderate to significant antioxidant profile. Statistical analysis also validated the experimental outcomes of biological activities. In conclusion, these synthesized and studied isatin metal-derived compounds stand out as potential candidates in developing effective drugs against microbial infection.

Supplementary Information The online version contains supplementary material available at https://doi.org/10.1007/s11696-022-02123-1.

Acknowledgements The authors thank the Higher Education Commission (HEC), Islamabad, Pakistan, for financial assistance through NRPU Project # 7800. The authors extend their appreciation to the Deanship of Scientific Research at King Khalid University for funding this work through research groups program under grant number R.G.P.2/40/43.

Declarations

Conflict of interest The authors declare no any conflict of interest regarding the publication of this paper.

References

Akman F, Issaoui N, Kazachenko AS (2020) Intermolecular hydrogen bond interactions in the thiourea/water complexes (Thio-(H_2O) n)(n = 1,…, 5): X-ray, DFT, NBO, AIM, and RDG analyses. J Mol Model 26:1–16. https://doi.org/10.1007/s00894-020-04423-3

Al-Amiery AA, Al-Bayati RI, Saed FM, Ali WB, Kadhum AAH, Mohamad AB (2012) Novel pyranopyrazoles: Synthesis and theoretical studies. Molecules 17:10377–10389. https://doi.org/10.3390/molecules170910377

Al-Hazmi GA, Abou-Melha KS, El-Metwaly NM, Althagafi I, Shaaban F, Elghalban MG, El-Gamil MM (2020) Spectroscopic and theoretical studies on Cr(III), Mn(II) and Cu(II) complexes of hydrazone derived from picolinic hydrazide and *o*-vanillin and evaluation of biological potency. Appl Organomet Chem 34:e5408. https://doi.org/10.1002/aoc.5408

Altürk S, Avcı D, Tamer Ö, Atalay Y (2017) Comparison of different hybrid DFT methods on structural, spectroscopic, electronic and NLO parameters for a potential NLO material. Comput Theor Chem 1100:34–45. https://doi.org/10.1016/j.comptc.2016.12.007

Arivazhagan M, Manivel S, Jeyavijayan S, Meenakshi R (2015) Vibrational spectroscopic (FTIR and FT-Raman), first-order hyperpolarizablity, HOMO, LUMO, NBO, Mulliken charge analyses of 2-ethylimidazole based on Hartree-Fock and DFT calculations. Spectrochim Acta A Mol Biomol Spectrosc 134:493–501. https://doi.org/10.1016/j.saa.2014.06.108

Arunachalam S, Priya NP, Boopathi K, Jayabalakrishnan C, Chinnusamy V (2010) Biocidal and catalytic efficiency of ruthenium(III) complexes with tridentate Schiff base ligands. Appl Organomet Chem 24:491–498. https://doi.org/10.1002/aoc.1647

Bakır TK, Lawag JB (2020) Preparation, characterization, antioxidant properties of novel Schiff bases including 5-chloroisatin-thiocarbohydrazone. Res Chem Intermed 46:2541–2557. https://doi.org/10.1007/s11164-020-04105-y

Bashiri M, Jarrahpour A, Nabavizadeh SM, Karimian S, Rastegari B, Haddadi E, Turos E (2021) Potent antiproliferative active agents: Novel bis Schiff bases and bis spiro β-lactams bearing isatin tethered with butylene and phenylene as spacer and DNA/BSA binding behavior as well as studying molecular docking. Med Chem Res 30(1):258–284. https://doi.org/10.1007/s00044-020-02659-5

Brandão P, Marques C, Burke AJ, Pineiro M (2020) The application of isatin-based multicomponent-reactions in the quest for new bioactive and drug like molecules. Eur J Med Chem 211:113102. https://doi.org/10.1016/j.ejmech.2020.113102

Brémond ÉA, Kieffer J, Adamo C (2010) A reliable method for fitting TD-DFT transitions to experimental UV–visible spectra. J Mol Struct THEOCHEM 954:52–56. https://doi.org/10.1016/j.theochem.2010.04.038

Chandrasekar T, Arunadevi A, Raman N (2021) Synthesis, spectral characterization, DNA-binding and antimicrobial profile of biological active mixed ligand Schiff base metal(II) complexes incorporating 1,8-diaminonaphthalene. J Coord Chem 74:1–19. https://doi.org/10.1080/00958972.2020.1870967

Chohan ZH, Sumrra SH, Youssoufi MH, Hadda TB (2010) Metal based biologically active compounds: Design, synthesis, and antibacterial/antifungal/cytotoxic properties of triazole-derived Schiff bases and their oxovanadium(IV) complexes. Eur J Med Chem 45:2739–2747. https://doi.org/10.1016/j.ejmech.2010.02.053

Dar OA, Lone SA, Malik MA, Aqlan FM, Wani MY, Hashmi AA, Ahmad A (2019) Synthesis and synergistic studies of isatin based mixed ligand complexes as potential antifungal therapeutic agents. Heliyon 5:e02055. https://doi.org/10.1016/j.heliyon.2019.e02055

De Moraes GPAT, Pena LJ, Leite ACL (2019) Isatin derivatives and their antiviral properties against arboviruses: A review. Mini-Rev Med Chem 19:56–62. https://doi.org/10.2174/1389557518666180424093305

Dennington R, Keith T, Millam J (2009) GaussView, Version 5. Semichem Inc, Shawnee Mission, KS

Dharsini GP, Thanaraj C, Velladurai R (2020) Metal chelates of tridentate (NNO) 1,2,4-triazine Schiff base: Synthesis, physicochemical investigation and pharmacological screening. J Inorg Organomet Polym Mater 30:2315–2322. https://doi.org/10.1007/s10904-019-01413-8

Ejidike IP, Ajibade PA (2015) Synthesis, characterization and biological studies of metal(II) complexes of (3*E*)-3-[(2-{(*E*)-[1-(2,4-dihydroxyphenyl)ethylidene] amino}ethyl)imino]-1-phenylbutan-1-one Schiff base. Molecules 20:9788–9802. https://doi.org/10.3390/molecules20069788

Ejidike IP, Ajibade PA (2016) Synthesis, characterization, anticancer, and antioxidant studies of Ru(III) complexes of monobasic tridentate Schiff bases. Bioinorg Chem Appl 2016:9672451. https://doi.org/10.1155/2016/9672451

Frisch M, Trucks G, Schlegel HB, Scuseria GE, Robb MA, Cheeseman JR, Scalmani G, Barone V, Mennucci B, Petersson G (2009) Gaussian 09, revision D. 01. Gaussian Inc, Wallingford CT: 20:307–309

González A, Quirante J, Nieto J, Almeida MR, Saraiva MJ, Planas A, Arsequell G, Valencia G (2009) Isatin derivatives, a novel class of transthyretin fibrillogenesis inhibitors. Bioorg Med Chem Lett 19:5270–5273. https://doi.org/10.1016/j.bmcl.2009.03.004

Grivani G, Bruno G, Rudbari HA, Khalaji AD, Pourteimouri P (2012) Synthesis, characterization and crystal structure determination of a new oxovanadium(IV) Schiff base complex: The catalytic activity in the epoxidation of cyclooctene. Inorg Chem Commun 18:15–20. https://doi.org/10.1016/j.inoche.2011.12.044

Guo H (2019) Isatin derivatives and their anti-bacterial activities. Eur J Med Chem 164:678–688. https://doi.org/10.1016/j.ejmech.2018.12.017

Hanif M, Chohan ZH (2013) Design, spectral characterization and biological studies of transition metal(II) complexes with triazole Schiff bases. Spectrochim Acta A Mol Biomol Spectrosc 104:468–476. https://doi.org/10.1016/j.saa.2012.11.077

Hassan AU, Sumrra SH (2021) Exploring the bioactive sites of new sulfonamide metal chelates for multi-drug resistance: An experimental versus theoretical design. J Inorg Organomet Polym Mater. https://doi.org/10.1007/s10904-021-02135-6

Hassan AU, Sumrra SH, Raza MA, Zubair M, Zafar MN, Mughal EU, Nazar MF, Irfan A, Imran M, Assiri MA (2021) Design, facile synthesis, spectroscopic characterization, and medicinal probing of metal-based new sulfonamide drugs: A theoretical and spectral study. Appl Organomet Chem 35:e6054. https://doi.org/10.1002/aoc.6054

Havrylyuk D, Zimenkovsky B, Vasylenko O, Gzella A, Lesyk R (2012) Synthesis of new 4-thiazolidinone-, pyrazoline-, and isatin-based conjugates with promising antitumor activity. J Med Chem 55:8630–8641. https://doi.org/10.1021/jm300789g

Ibrahim HS, Abou-Seri SM, Abdel-Aziz HA (2016) 3-Hydrazinoindolin-2-one derivatives: Chemical classification and investigation of their targets as anticancer agents. Eur J Med Chem 122:366–381. https://doi.org/10.1016/j.ejmech.2016.06.034

Ismail BA, Nassar DA, Abd El–Wahab ZH, Ali OA, (2021) Synthesis, characterization, thermal, DFT computational studies and anticancer activity of furfural-type Schiff base complexes. J Mol Struct 1227:129393. https://doi.org/10.1016/j.molstruc.2020.129393

Issa TB, Sagaama A, Issaoui N (2020) Computational study of 3-thiophene acetic acid: Molecular docking, electronic and intermolecular interactions investigations. Comput Biol Chem 86:107268. https://doi.org/10.1016/j.compbiolchem.2020.107268

Issaoui N, Rekik N, Oujia B, Wójcik MJ (2009) Anharmonic effects on theoretical IR line shapes of medium strong H (D) bonds. Int J Quantum Chem 109:483–499. https://doi.org/10.1002/qua.21839

Issaoui N, Rekik N, Oujia B, Wójcik MJ (2010) Theoretical infrared line shapes of H-bonds within the strong anharmonic coupling theory and Fermi resonances effects. Int J Quantum Chem 110:2583–2602. https://doi.org/10.1002/qua.22395

Jomaa I, Noureddine O, Gatfaoui S, Issaoui N, Roisnel T, Marouani H (2020) Experimental, computational, and *in silico* analysis of $(C_8H_{14}N_2)_2[CdCl_6]$ compound. J Mol Struct 1213:128186. https://doi.org/10.1016/j.molstruc.2020.128186

Kakkar R (2019) Isatin and its derivatives: A survey of recent syntheses, reactions, and applications. MedChemComm 10(3):351–368. https://doi.org/10.1039/C8MD00585K

Kargar H, Ardakani AA, Munawar KS, Ashfaq M, Tahir MN (2021) Nickel(II), copper(II) and zinc(II) complexes containing symmetrical tetradentate Schiff base ligand derived from 3,5-diiodosalicylaldehyde: Synthesis, characterization, crystal structure and antimicrobial activity. J Iran Chem Soc. https://doi.org/10.1007/s13738-021-02207-x

Kaur S, Modi NH, Panda D, Roy N (2010) Probing the binding site of curcumin in *Escherichia coli* and *Bacillus subtilis* FtsZ–a structural insight to unveil antibacterial activity of curcumin. Eur J Med Chem 45:4209–4214. https://doi.org/10.1016/j.ejmech.2010.06.015

Keeling KB, Pavur RJ (2007) A comparative study of the reliability of nine statistical software packages. Comput Stat Data Anal 51:3811–3831. https://doi.org/10.1016/j.csda.2006.02.013

Khalid S, Sumrra SH, Chohan ZH (2020) Isatin endowed metal chelates as antibacterial and antifungal agents. Sains Malays 49:1891–1904. https://doi.org/10.17576/jsm-2020-4908-11

Li W, Zhao SJ, Gao F, Lv ZS, Tu JY, Xu Z (2018) Synthesis and *in vitro* anti-tumor, anti-mycobacterial and anti-HIV activities of diethylene-glycol-tethered bis-isatin derivatives. Chemistry Select 3:10250–10254. https://doi.org/10.1002/slct.201802185

Maurya RC, Sutradhar D, Martin MH, Roy S, Chourasia J, Sharma AK, Vishwakarma P (2015) Oxovanadium(IV) complexes of medicinal relevance: Synthesis, characterization, and 3D-molecular modeling and analysis of some oxovanadium(IV) complexes in O, N-donor coordination matrix of sulfa drug Schiff bases derived from a 2-pyrazolin-5-one derivative. Arab J Chem 8:78–92. https://doi.org/10.1016/j.arabjc.2011.01.009

Mermer A, Bayrak HACER, Alyar S, Alagumuthu M (2020) Synthesis, DFT calculations, biological investigation, molecular docking studies of β-lactam derivatives. J Mol Struct 1208:127891. https://doi.org/10.1016/j.molstruc.2020.127891

Mitra M, Seth SK, Choudhury SR, Manna P, Das A, Helliwell M, Bauzá A, Frontera A, Mukhopadhyay S (2013) MII–malonate complexes (M = Mg, Cu, Ni and Co) characterized by layered structures: Experimental observation, Hirshfeld surface analysis and theoretical study. Eur J Inorg Chem 2013:4679–4685. https://doi.org/10.1002/ejic.201300459

Nagesh GY, Mruthyunjayaswamy BHM (2015) Synthesis, characterization and biological relevance of some metal(II) complexes with oxygen, nitrogen and oxygen (ONO) donor Schiff base ligand derived from thiazole and 2-hydroxy-1-naphthaldehyde. J Mol Struct 1085:198–206. https://doi.org/10.1016/j.molstruc.2014.12.058

Noreen S, Sumrra SH (2021) Aminothiazole-linked metal chelates: Synthesis, density functional theory, and antimicrobial studies with antioxidant correlations. ACS Omega 6(48):33085–33099. https://doi.org/10.1021/acsomega.1c05290

Ouari K, Bendia S, Weiss J, Bailly C (2015) Spectroscopic, crystal structural and electrochemical studies of zinc(II)-Schiff base complex obtained from 2,3-diaminobenzene and 2-hydroxy naphthaldehyde. Spectrochim Acta A Mol Biomol Spectrosc 135:624–631. https://doi.org/10.1016/j.saa.2014.07.034

Pedreño E, López-Contreras AJ, Cremades A, Peñafiel R (2005) Protecting or promoting effects of spermine on DNA strand breakage induced by iron or copper ions as a function of metal concentration. J Inorg Biochem 99:2074–2080. https://doi.org/10.1016/j.jinorgbio.2005.07.005

Penthala NR, Yerramreddy TR, Madadi NR, Crooks PA (2010) Synthesis and *in vitro* evaluation of *N*-alkyl-3-hydroxy-3-(2-imino-3-methyl-5-oxoimidazolidin-4-yl)indolin-2-one analogs as potential anticancer agents. Bioorg Med Chem Lett 20:4468–4471. https://doi.org/10.1016/j.bmcl.2010.06.042

Pervez H, Ahmad M, Zaib S, Yaqub M, Naseer MM, Iqbal J (2016) Synthesis, cytotoxic and urease inhibitory activities of some novel Isatin-derived Bis-Schiff bases and their copper(II) complexes. MedChemComm 7(5):914–923. https://doi.org/10.1039/C5MD00529A

Prabavathi N, Nilufer A, Krishnakumar V (2014) FT-IR, FT-Raman and DFT quantum chemical study on the molecular conformation, vibrational and electronic transitions of 1-(*m*-(trifluoromethyl) phenyl)piperazine. Spectrochim Acta A Mol Biomol Spectrosc 121:483–493. https://doi.org/10.1016/j.saa.2013.10.102

Rekik N, Issaoui N, Ghalla H, Oujia B, Wójcik MJ (2007a) IR spectral density of H-bonds. Both intrinsic anharmonicity of the fast mode and the H-bond bridge. Part I: Anharmonic coupling parameter and temperature effects. J Mol Struct Theochem 821:9–21. https://doi.org/10.1016/j.theochem.2007.06.016

Rekik N, Issaoui N, Ghalla H, Oujia B, Wójcik MJ (2007b) Infrared spectral density of H-bonds within the strong anharmonic coupling theory: Indirect relaxation effect. J Mol Struct 844:21–31. https://doi.org/10.1016/j.molstruc.2007.02.040

Sagaama A, Issaoui N (2020) Design, molecular docking analysis of an anti-inflammatory drug, computational analysis and intermolecular interactions energy studies of 1-benzothiophene-2-carboxylic acid. Comput Biol Chem 88:107348. https://doi.org/10.1016/j.compbiolchem.2020.107348

Sakthikumar K, Raja JD, Solomon RV, Sankarganesh M (2019) Density functional theory molecular modelling, DNA interactions, antioxidant, antimicrobial, anticancer and biothermodynamic studies of bioactive water-soluble mixed ligand complexes. J Biomol Struct Dyn 37:2498–2514. https://doi.org/10.1080/07391102.2018.1492970

Shakir M, Hanif S, Sherwani MA, Mohammad O, Azam M, Al-Resayes SI (2016) Pharmacophore hybrid approach of new modulated bis-diimine CuII/ZnII complexes based on 5-chloro isatin Schiff base derivatives: Synthesis, spectral studies and comparative biological assessment. J Photochem Photobiol B Biol 157:39–56. https://doi.org/10.1016/j.jphotobiol.2016.01.019

Sonmez F, Gunesli Z, Kurt BZ, Gazioglu I, Avci D, Kucukislamoglu M (2019) Synthesis, antioxidant activity and SAR study of novel spiro-isatin-based Schiff bases. Mol Divers 23:829–844. https://doi.org/10.1007/s11030-018-09910-7

Srivastava AK, Misra N (2014) A comparative theoretical study on the biological activity, chemical reactivity, and coordination ability of dichloro-substituted (1,3-thiazol-2-yl)acetamides. Can J Chem 92:234–239. https://doi.org/10.1139/cjc-2013-0335

Sumrra SH, Hanif M, Chohan ZH, Akram MS, Akhtar J, Al-Shehri SM (2016) Metal based drugs: Design, synthesis and *in-vitro* antimicrobial screening of Co(II), Ni(II), Cu(II) and Zn(II) complexes with some new carboxamide derived compounds: Crystal structures of N-[ethyl(propan-2-yl)carbamothioyl]thiophene-2-carboxamide and its copper(II) complex. J Enzyme Inhib Med Chem 31:590–598. https://doi.org/10.3109/14756366.2015.1050011

Sumrra SH, Kausar S, Raza MA, Zubair M, Zafar MN, Nadeem MA, Mughal EU, Chohan ZH, Mushtaq F, Rashid U (2018) Metal based triazole compounds: Their synthesis, computational,

antioxidant, enzyme inhibition and antimicrobial properties. J Mol Struct 1168:202–211. https://doi.org/10.1016/j.molstruc.2018.05.036

Sumrra SH, Habiba U, Zafar W, Imran M, Chohan ZH (2020) A review on the efficacy and medicinal applications of metal-based triazole derivatives. J Coord Chem 73:2838–2877. https://doi.org/10.1080/00958972.2020.1839751

Sumrra SH, Arshad Z, Zafar W, Mahmood K, Ashfaq M, Hassan AU, Mughal EU, Irfan A, Imran M (2021a) Metal incorporated aminothiazole-derived compounds: synthesis, density function theory analysis, *in vitro* antibacterial and antioxidant evaluation. R Soc Open Sci 8:210910. https://doi.org/10.1098/rsos.210910

Sumrra SH, Zafar W, Javed H, Zafar M, Hussain MZ, Imran M, Nadeem MA (2021b) Facile synthesis, spectroscopic evaluation and antimicrobial screening of metal endowed triazole compounds. Biometals 34(6):1329–1351. https://doi.org/10.1007/s10534-021-00345-6

Sumrra SH, Zafar W, Malik SA, Mahmood K, Shafqat SS, Arif S (2021c) Metal based bioactive nitrogen and oxygen donor mono and bis Schiff bases: Design, synthesis, spectral characterization, computational analysis and antibacterial screening. Acta Chim Slov. https://doi.org/10.17344/acsi.2021.7182

Weinhold F, Landis CR, Glendening ED (2016) What is NBO analysis and how is it useful? Int Rev Phys Chem 35:399–440. https://doi.org/10.1080/0144235X.2016.1192262

Yakan H, Bakır TK, Çavuş MS, Muğlu H (2020) New β-isatin aldehyde-N, N′-thiocarbohydrazones: Preparation, spectroscopic studies and DFT approach to antioxidant characteristics. Res Chem Intermed 46:5417–5440. https://doi.org/10.1007/s11164-020-04270-0

Zafar W, Sumrra SH, Chohan ZH (2021) A review: Pharmacological aspects of metal based 1,2,4-triazole derived Schiff bases. Eur J Med Chem 222:113602. https://doi.org/10.1016/j.ejmech.2021.113602